NASA/TM–2020-220435

Simulation of a Full-Scale Crash Test of a Fokker F28 Fellowship Aircraft

Karen E. Jackson
National Institute of Aerospace, Hampton, Virginia

Jacob B. Putnam
Langley Research Center, Hampton, Virginia

February 2020

NASA STI Program . . . in Profile

Since its founding, NASA has been dedicated to the advancement of aeronautics and space science. The NASA scientific and technical information (STI) program plays a key part in helping NASA maintain this important role.

The NASA STI program operates under the auspices of the Agency Chief Information Officer. It collects, organizes, provides for archiving, and disseminates NASA's STI. The NASA STI program provides access to the NTRS Registered and its public interface, the NASA Technical Reports Server, thus providing one of the largest collections of aeronautical and space science STI in the world. Results are published in both non-NASA channels and by NASA in the NASA STI Report Series, which includes the following report types:

- TECHNICAL PUBLICATION. Reports of completed research or a major significant phase of research that present the results of NASA Programs and include extensive data or theoretical analysis. Includes compilations of significant scientific and technical data and information deemed to be of continuing reference value. NASA counter-part of peer-reviewed formal professional papers but has less stringent limitations on manuscript length and extent of graphic presentations.

- TECHNICAL MEMORANDUM. Scientific and technical findings that are preliminary or of specialized interest, e.g., quick release reports, working papers, and bibliographies that contain minimal annotation. Does not contain extensive analysis.

- CONTRACTOR REPORT. Scientific and technical findings by NASA-sponsored contractors and grantees.

- CONFERENCE PUBLICATION. Collected papers from scientific and technical conferences, symposia, seminars, or other meetings sponsored or co-sponsored by NASA.

- SPECIAL PUBLICATION. Scientific, technical, or historical information from NASA programs, projects, and missions, often concerned with subjects having substantial public interest.

- TECHNICAL TRANSLATION. English-language translations of foreign scientific and technical material pertinent to NASA's mission.

Specialized services also include organizing and publishing research results, distributing specialized research announcements and feeds, providing information desk and personal search support, and enabling data exchange services.

For more information about the NASA STI program, see the following:

- Access the NASA STI program home page at http://www.sti.nasa.gov

- E-mail your question to help@sti.nasa.gov

- Phone the NASA STI Information Desk at 757-864-9658

- Write to:
  NASA STI Information Desk
  Mail Stop 148
  NASA Langley Research Center
  Hampton, VA 23681-2199

NASA/TM–2020-220435

Simulation of a Full-Scale Crash Test of a Fokker F28 Fellowship Aircraft

Karen E. Jackson
National Institute of Aerospace, Hampton, Virginia

Jacob B. Putnam
Langley Research Center, Hampton, Virginia

National Aeronautics and
Space Administration

Langley Research Center
Hampton, Virginia 23681-2199

February 2020

Available from:

NASA STI Program / Mail Stop 148
NASA Langley Research Center
Hampton, VA 23681-2199
Fax: 757-864-6500

1.0 ABSTRACT

In June 2019, a full-scale crash test of a Fokker F28 Fellowship aircraft was conducted as part of a joint National Aeronautics and Space Administration/Federal Aviation Administration (NASA/FAA) project to investigate the performance of transport aircraft under realistic crash conditions. The test objectives were to provide data for assessment of transport aircraft crashworthiness and to generate test data for model validation. The test article was loaded with transport aircraft seats in a 3+2 configuration. A total of 24 instrumented Anthropomorphic Test Devices (ATDs) were placed in the seats and restrained. The test article weighed 33,306-lb. and, during the crash test, impacted a 2-ft. high soil bed at 65.3-ft/s forward and 31.8-ft/s vertical velocity. The full-scale crash test was simulated using the commercial nonlinear explicit transient dynamic finite element code, LS-DYNA®. This paper will provide a description of the test article and the crash test conditions, document the F28 full-scale model development, and present test-analysis comparisons in several categories including inertial properties, kinematic responses, structural acceleration responses, and airframe deformation and failure. In addition, test-analysis results will be quantified based on the International Organization for Standardization (ISO) 16250 curve comparison methodology.

2.0 INTRODUCTION

An Inter-Agency Agreement (IAA) was signed between the National Aeronautics and Space Administration (NASA) Langley Research Center and the Federal Aviation Administration (FAA) in September 2016, to create a cooperative research effort to obtain data through a series of tests that support the development of airframe level crash requirements for transport category airplanes [1]. A retired Fokker F28 Fellowship aircraft, along with two sets of wings and three fuselage sections (two forward sections and a wing-box section), were obtained during the NASA Aviation Safety Program in 2000 [2]. The F28 is a high-performance twin-turbo fan narrow-body aircraft with seating in a 3+2 configuration. The F28 was first type certified by the FAA in 1969 and the F28 fleet has retired from service in the United States. A photograph of the aircraft arriving at Langley field is shown in Figure 1. Following arrival, all useful interior structures and equipment including avionics and other electronics, seats, and hat racks were removed. All fuel lines were drained, and the engines were also removed.

Figure 1. A photograph of the F28 aircraft after landing at Langley Field.

Only a small number of full-scale crash tests have been conducted on modern transport category aircraft (i.e. semi-monocoque with turbofan or turbojet engines capable of seating 20 or more passengers) due to the complexity of test setup, and scarcity of available aircraft. In the horizontal direction, a set of three tests were conducted at NASA Glenn Research Center [3] in 1958 using a linear accelerator impacting into berm surfaces to investigate accelerations experienced in the airframe during impact. In the vertical direction, the FAA has conducted drop tests of full-scale aircraft, including an ATR42-300 [4, 5], Metro III [6], Beechcraft 1900C [7] and a Shorts 3-30 [8] for the evaluation of airframe crashworthiness and occupant survivability during crash impacts of real aircraft.

Prior to the F28 test, only two full-scale crash tests of transport aircraft had been conducted under combined forward and vertical velocity impact conditions. The first was a joint FAA/NASA test conducted at Edwards Air Force Base in 1984 of a remotely piloted Boeing 720 aircraft and was known as the Controlled Impact Demonstration (CID) [9]. The primary objective of this test was to study a fuel additive, known as Anti Misting Kerosene (AMK), and its abilities to suppress a fuel fire following a crash. A second objective, which was led by a team of researchers at NASA Langley, was to examine occupant and seat/airframe responses for the evaluation of crashworthiness and occupant injury [10]. This test ended with the aircraft catching fire upon impact due to one of the wing cutters being ingested by the number 3 engine. Even with the fire, the majority of the crash test data was successfully telemetered to a remote site and analyzed. Prior to the CID test, NASA Langley conducted three vertical drop tests of Boeing 707 fuselage sections, as a means of fine tuning the data acquisition system for the CID and to generate additional data for model validation [11-13].

More recently, a crash test was conducted in 2012 for the Discovery channel show *Curiosity*, in which a Boeing 727-200 was crashed into the Mexican desert to evaluate impact loads on the airframe and to assess occupant survivability [14]. For this test, the pilot jumped out of the aircraft at a designated

altitude and landed safely under parachute. Meanwhile the aircraft descended and eventually crashed into the ground. Airframe and occupant loads were acquired for several onboard Anthropomorphic Test Devices (ATDs); however, video data is sparse since the aircraft impacted outside of the intended impact zone.

Three F28 fuselage sections have been subjected to vertical drop testing at the NASA Langley Research Center's Landing and Impact Research (LandIR) Facility [15]. The portions of the airframe from which the sections were taken are highlighted in the schematic drawing shown in Figure 2. The test of the first forward section was performed in 2001 [16, 17]. A photograph of this fuselage section is shown in a pre-test configuration in Figure 3(a). The section is 4.9 ft. long and 10.8-ft. in diameter. Twenty 75-lb. bars were attached to the seat rails to approximate the weight of the seats and occupants. The bars were placed symmetrically, 10 per side, and were incorporated to minimize any additional structural complexity and to simplify model development. The test was conducted using the 70-ft drop tower at LandIR onto concrete. To attain a purely vertical impact velocity of 30.2-ft/s, the section was released from a height of 14.1-ft. The velocity was selected to reflect an aircraft undergoing a severe, but survivable, vertical impact.

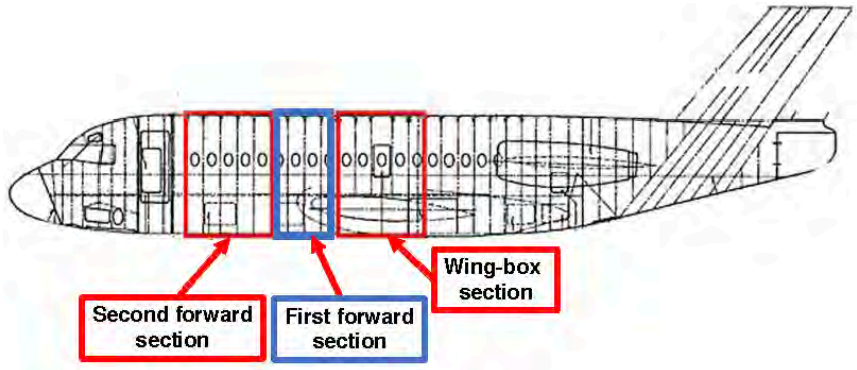

Figure 2. Side-view schematic of the F-28 highlighting the locations of three fuselage sections.

Vertical drop tests were conducted in March and June 2017 of the second forward and wing-box sections, respectively. These sections are shown pre-test in Figure 3(b) and (c), respectively. The forward section was tested at a 28.9-ft/s vertical velocity with a level pitch onto a soil bed. Note that the cargo hold of the forward section was filled with packed luggage. In contrast, the wing-box section impacted a graded soil bed with a downward pitch angle of 2.9°. The measured impact velocity was 29.1-ft/s. The wing-box section impacted a mound of soil that was placed over the concrete pad located at the LandIR facility. The soil was formed into a 20-ft by 20-ft square mound, with a downward facing 10° slope, such that the rear portion of the test article would contact first, causing a rotational velocity component about the rear impact point. This rotation would cause the forward portion of the test article to impact at a downward pitch angle. The rotation was intended to

induce a forward acceleration into the onboard ATDs. These two tests were designed to evaluate the proposed crashworthiness requirements on realistic aircraft components, as well as to perform detailed test-analysis comparisons [18, 19].

Post-test photographs of the three fuselage sections are shown in Figure 4. The first forward section exhibited discrete failures of the lower frames and skin at the point of impact, along the centerline, and at the location of the angled strut supports, as shown in Figure 4(a). This failure pattern was expected since the cargo hold was empty. In contrast, the second forward section contained luggage in the cargo hold, which prevented the drastic failures that were seen in the first forward section, as shown in Figure 4(b). Instead, the subfloor area of the forward section showed plastic deformation, rather than discrete failures. However, some failures were observed among the floor frames. The wing-box section, shown in Figure 4(c), exhibited only very minor failures of some structures located beneath the floor. In general, the airframe remained completely intact, despite multiple seat failures. Additional information on these tests can be found in References 20 and 21.

(a) First forward section. (b) Second forward section. (c) Wing-box section.

Figure 3. Pre-test photographs of three fuselage sections that were drop tested at NASA Langley.

The full-scale crash test of the F28 aircraft was conducted on June 20, 2019. The specific objectives of the test were: (1) To compare and contrast responses in identical aircraft undergoing vertical only to combined vertical and horizontal loading conditions, (2) To examine the effects of horizontal loading on aircraft structure during a crash event, (3) To generate data for calibration of computer simulations, (4) To generate data from onboard ATDs for the evaluation of injury, and (5) To obtain data from new and novel ATDs including Warrior Injury Assessment Manikin (WIAMan) [22], Test device for Human Occupant Restraint (THOR) [23], and others including several child ATDs. This document will present a description of the test article and crash test; a summary of the finite element model development; and test-analysis comparisons in several categories including inertial properties, kinematic responses, structural acceleration responses, and airframe deformation and failure. Where

possible, test-analysis results will be quantified based on the International Standards Organization (ISO) 16250 curve comparison methodology [24].

(a) First forward section. (b) Second forward section. (c) Wing-box section.

Figure 4. Post-test photographs of three F28 fuselage sections that were drop tested at NASA Langley.

3.0 DESCRIPTION OF THE TEST ARTICLE AND THE FULL-SCALE CRASH TEST

A complete F28 Fellowship (MK1000 variant) aircraft was obtained by the Aviation Safety Program at NASA Langley Research Center in 2000. Upon arrival, the aircraft was inspected and found to be structurally complete. There was flooring in the cabin; however, the overhead hat racks, seats, and some of the interior paneling had been removed. Figure 5 shows a photograph of the interior of the F28 aircraft, after removal of all useful equipment by the airline (CanadaAir) technicians.

The aircraft is 89 ft. in length and has a wingspan of 77-ft. The standard 3+2 seat configuration for this aircraft was used. Thirteen rows of seats can accommodate up to 65 passengers; however, only 24 ATDs were used during the test. Luggage was included in the form of foam ballast. Foam properties were selected to match the stiffness properties obtained from dynamic luggage testing conducted in the summer of 2017 [25]. Luggage ballast was loaded into the forward cargo hold. Overhead bins were recreated by attaching channel beams and ballasting weight onto frame attachment points. Existing floor panels were reused. Transport aircraft seats removed from an in-service Boeing 737 were reconfigured for use in a triple-double configuration. For the double configuration, the window seat of a triple was removed to create a double, as shown in Figure 6. One issue created by this seating arrangement is that the aisle occupant in the triple seat is not directly supported but is instead cantilevered. The floor was ballasted using a combination of seated ATDs, and data acquisition systems. As much as possible, the loading conditions were dictated by the F28 weight and balance manual.

Figure 5. Interior view of the F28 aircraft, following removal of equipment by CanadaAir.

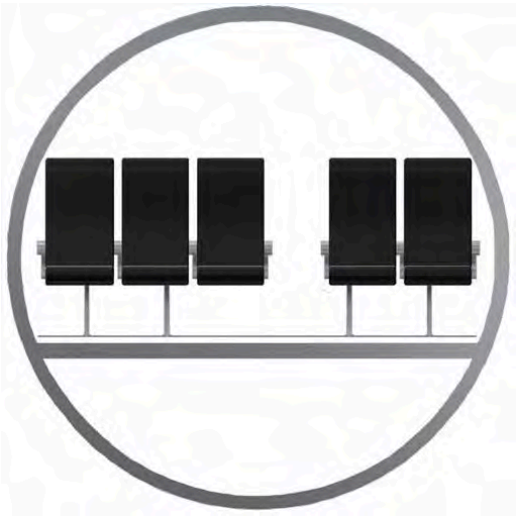

Figure 6. Schematic drawing of the 3+2 seat configuration.

Altogether, 363 channels of test data were collected using the NASA Data Acquisition System (DAS) including ATD responses, and structural responses at the seat bases, airframe/floor intersections, and discrete locations throughout the aircraft. The WIAMan dummy had a stand-alone DAS used to collect 278 separate channels. Finally, a separate DAS was used to collect data from one additional FAA dummy. NASA data were collected at 10,000 samples per second. Figure 7 shows the location of airframe/floor channels, depicted as blue triangles, on a schematic of the aircraft. These accelerometers were located on the frame webs, approximately 1-2-inches above the floor, as shown in Figure 8(a). The seat base accelerometers were located near the seat attachment with the seat rail, as shown in Figure 8(b).

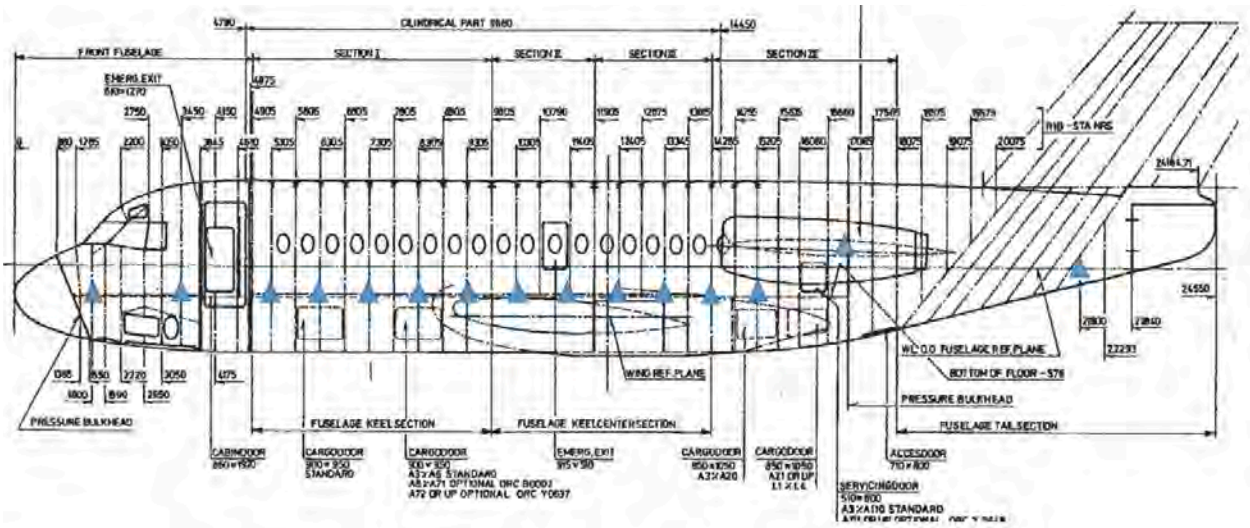

Figure 7. Schematic of the F28 aircraft showing the locations of airframe/floor accelerometers.

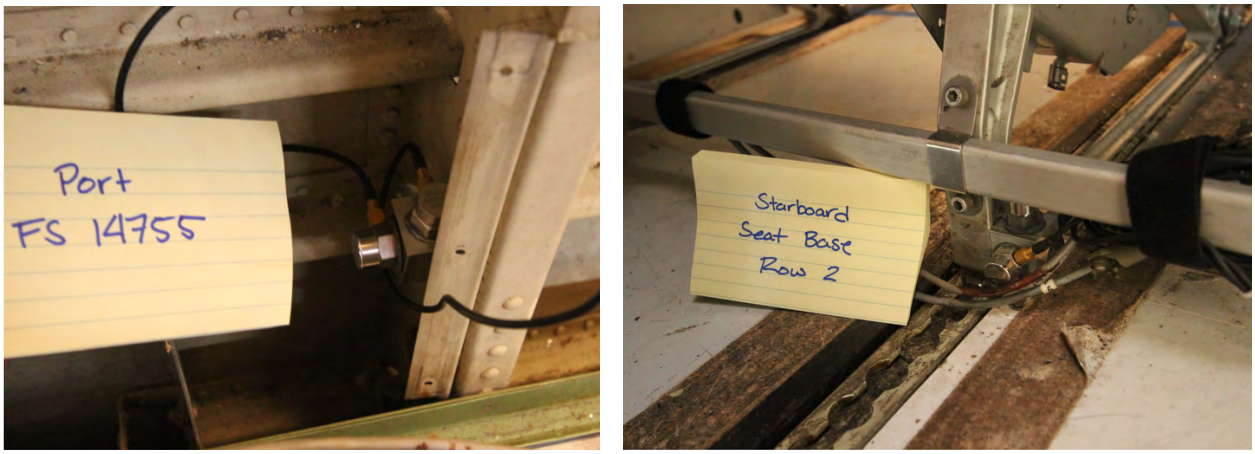

(a) Accelerometer located at the airframe/floor. (b) Accelerometer located at the seat base.

Figure 8. Photographs illustrating the location of airframe/floor and seat base accelerometers.

Prior to impact, a weight and balance test was performed of the fully loaded aircraft. Measured total weight was 33,306-lb. The Center-of-Gravity (CG) in the x-direction (longitudinal) was measured to be 455.0-in. from the tip of the nose. The CGy was located at 0.0-in., meaning that it fell on the lateral centerline of the aircraft. The CGz was measured to be -80-in. below the water line. Prior to the impact test, the port side of the airframe was painted white with randomly spaced 3-in. diameter black dots added for collecting 2-D and 3-D photogrammetric data, as shown in Figure 9. Photogrammetry is an extremely useful tool used to capture 2-D and 3-D motion of the targets, which can then be used to create fringe plots of deformation [26, 27].

The test article was loaded with 24 ATDs, as shown in Figure 10. These included two WIAMan dummies provided by the US Army Research Laboratory [22]. In addition, ATDs were obtained from the inventories of NASA, the FAA, the National Highway Traffic Safety Administration (NHTSA), and Humanetics.

Figure 9. Photograph of the F28 as it is being lifted to the drop height. Note that the port side was painted white with 3-in.-diameter black dots added for photogrammetry.

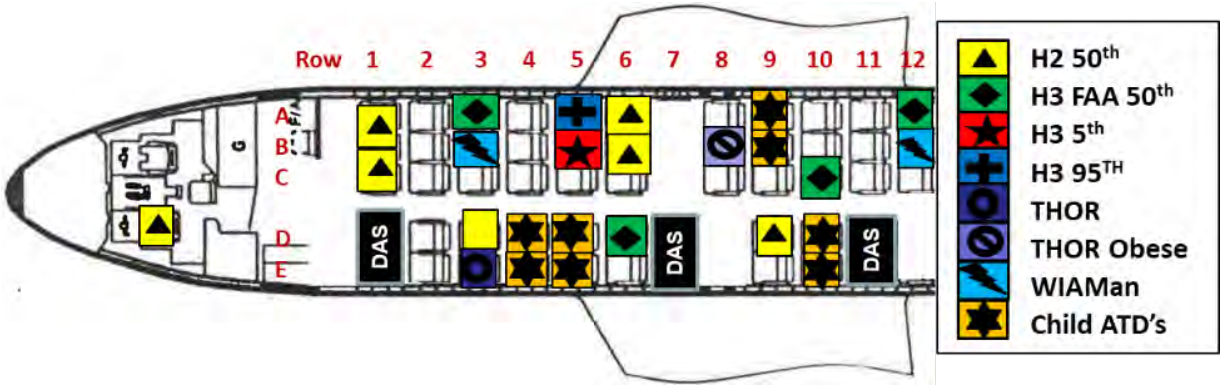

Figure 10. Layout of 24 ATDs in the F28 aircraft.

The full-scale crash test was conducted at NASA Langley's LandIR facility [15] onto a 2-ft. high soil bed. The soil was a mixture of sand and clay. The test was conducted by raising the aircraft using two sets of swing cables, arranged in a parallelogram configuration, and pullback cables. By using a parallelogram configuration of the swing cables, the creation of pitch angular acceleration is eliminated, as would normally be developed during a pendulum swing. Once the drop height is attained, the aircraft is released, following a countdown, and allowed to swing to the Earth. Just prior to impact, all remaining cables are pyrotechnically separated such that the aircraft hits the impact

surface without restraint. Measured impact conditions were: Forward Velocity = 65.3-ft/s (783.6-in/s), Vertical Velocity = 31.8-ft/s (381.6-in/s), and Lateral Velocity = 0.0=ft/s (0.0-in/s). Measured impact attitudes were: Pitch = 0.38° nose down, Roll = 4.3° starboard side down, and Yaw = 2.58° nose left. Additional information on the test set-up, instrumentation, camera coverage, and ATD layout can be found in Reference 28.

4.0 DEVELOPMENT OF THE LS-DYNA FINITE ELEMENT MODEL

When NASA purchased the F28 hardware in 2000, an existing NASTRAN [29] loads model of the aircraft was also purchased. This model is shown in Figure 11. The NASTRAN model was used for overall airframe geometry. Considerable work was expended to convert the model into a viable representation of the aircraft and into LS-DYNA format. This work included changing the system of units, adding elements to represent missing structures, and defining and reconnecting the mesh. LS-DYNA is a commercial software package, marketed by Livermore Software Technology Corporation (LSTC), and is used to perform nonlinear, explicit transient dynamic simulations of structures subjected to high speed impact [30-32]. The final model is depicted in Figure 12 and it contained: 255,794 nodes; 26,573 beam elements; 81,288 shell elements; 145,057 solid elements; 44 element masses; 76 Constrained Nodal Rigid Bodies (CNRBs); 77 material definitions; 746 parts; and 5 contact definitions. Several key features of the model are shown in Figure 12. Note that a rigid wall was located at the far end of the soil bed to prevent the aircraft from sliding into the Hydro Impact Basin at LandIR. In addition, two drag chains were mounted at the wing/fuselage attachment points on both sides of the aircraft. These chains allowed the aircraft to slide out approximately 20-ft. before it began pulling two 5,000-lb. weights. The drag chains were used to help slow the aircraft down following impact. In the model, the drag chains were represented using discrete springs with a defined load-displacement response.

Figure 11. NASTRAN loads model of the F28 aircraft.

The 2-ft. high soil bed was represented as a layered soil model. The top layer was assigned material properties of Gantry Unwashed Sand (GUS) using *MAT_SOIL_AND_FOAM (Mat 5) in LS-DYNA. The GUS soil properties had been previously studied, as described in References 33 and 34.

The bottom layer of soil was represented using soil properties for Carson Sink Wet, which is another soil that had been evaluated as a landing site for the Orion Crew Module [35, 36].

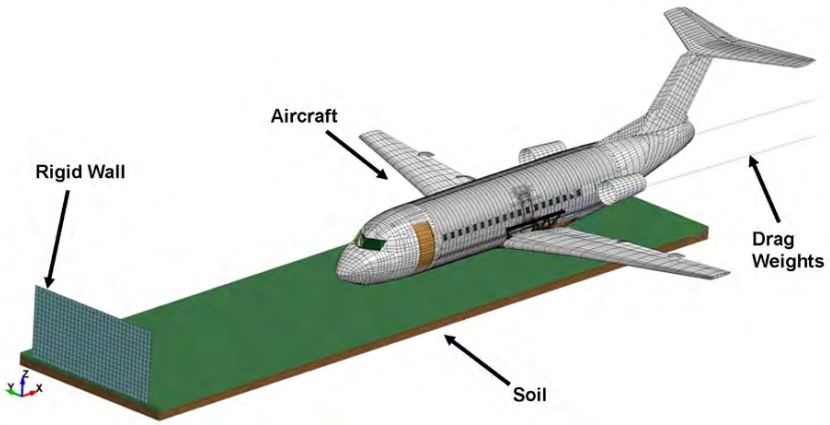

Figure 12. Overview depiction of the F28 aircraft model.

The seats and occupants were initially represented as concentrated masses that were attached to the seat rails using CNRBs, as shown in Figure 13. The seats, restraints, and ATD finite element models were simulated separately as individual occupant breakout models. The occupant simulation was broken out from the full vehicle model in this way to optimize simulation run time. The methods, results, and analysis of this modeling effort are described in Reference 37.

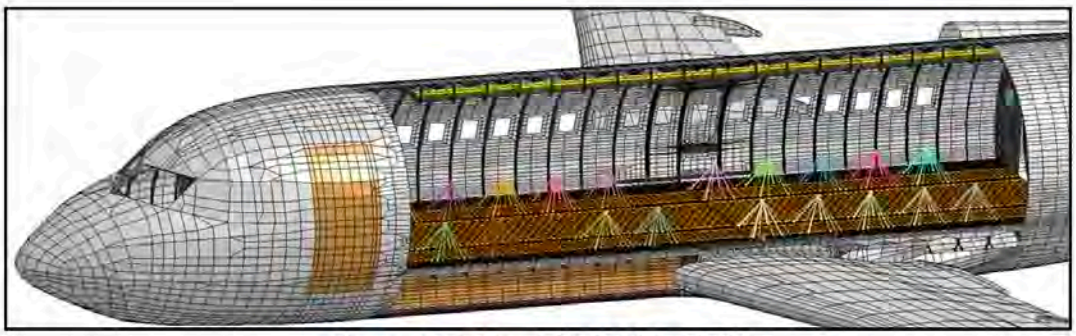

Figure 13. Representation of the seat/occupant masses.

In total, five different contact surfaces were defined in the model. One contact definition was written to prevent the forward portion of the aircraft from getting past the rigid wall. This contact was actually not needed since the aircraft never got close to hitting the wall. A second contact defined the interaction between the aircraft and the soil. This contact definition had static and dynamic coefficients of friction of 0.59. Additional contacts were used to define interactions between the foam in the cargo hold (used to represent luggage) and the outer fuselage surface, the floor, and the forward cargo hold.

Nodal output was requested for test-analysis comparisons at the seat bases, the airframe/floor intersections, and discrete locations including the nose bulkhead, the port and starboard engine nacelles, and the tail. The model was executed for 1.75-seconds on a Linux-based workstation computer with 8 processors, running LS-DYNA version R10.1.0 (double precision), which required 19 hours and 27 minutes of computational time.

5.0 TEST-ANALYSIS COMPARISONS

The test-analysis comparisons are categorized, as follows: inertial property comparisons; kinematic comparisons; structural acceleration comparisons; airframe deformation and failure; and, quantitative test-analysis correlation results.

5.1 Inertial Property Comparisons

As mentioned previously, a weight and balance test was performed on the fully loaded F28 aircraft prior to the crash test. A comparison of the test-analysis weight and balance is shown in Table 1. As indicated in the Table, the model weighs 354.6-lb. less than the test article. Please note that for this comparison, the soil was not included in the model calculations. The comparison with CG locations is excellent, and the maximum percentage difference between test and analysis is 6.6%.

Table 1. Comparison of Weight and Balance

Parameter	Model	Test	Difference, (Percentage)
Weight, lb.	32,951.4	33,306	354.6 (1.06%)
CGx, in.	449.5	455.0	5.5 (1.2%)
CGy, in.	0.89	0.0	0.89
CGz, in.	-85.3	-80.0	5.3 (6.6%)

5.2 Kinematic Comparisons

Kinematic comparisons between the test and analysis focus on the gross motion of the test article and model as the impact occurs including the timing of events and slide out of the vehicle. Photogrammetric analysis of the test indicated that the time required from initial contact until the airframe came to rest was 1.667-seconds. Plots of photogrammetric forward and vertical velocity data are shown in Figure 14. Position data was tracked for each of the targets and saved. It was then differentiated, and a 5-point moving average was applied to the data. There is a high amount of noise in the data due to the limited resolution of the tracking camera, even after the averaging filter has been applied. The data is plotted versus time after impact, in which the impact event occurs at T=0.

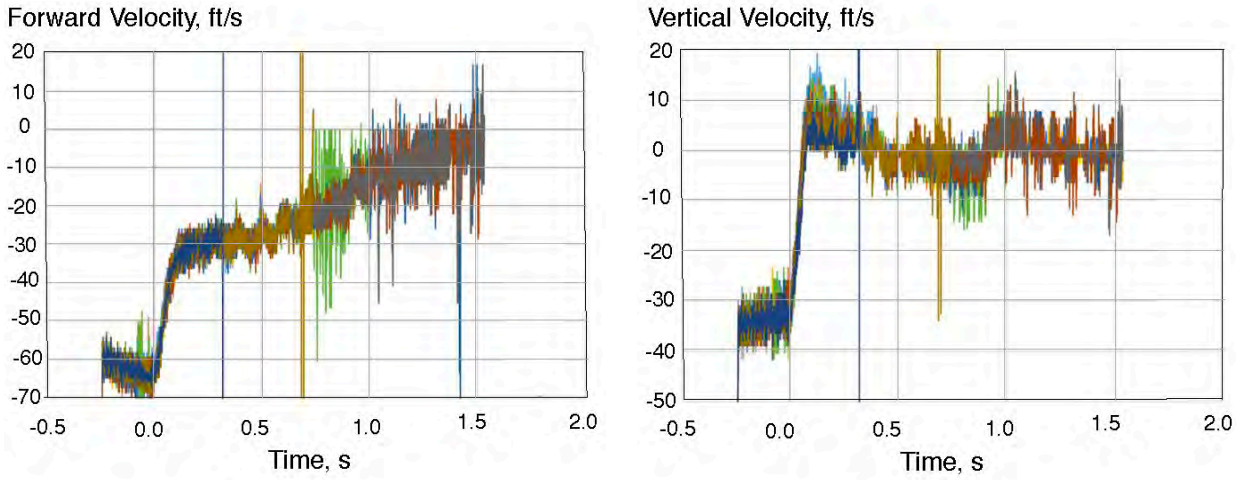

(a) Forward velocity responses. (b) Vertical velocity responses.

Figure 14. Photogrammetric data of forward and vertical velocities.

As a comparison, forward and vertical velocity responses of nodes on the surface of the model that approximate the location of targets used to collect photogrammetric data are shown in Figure 15 for the same time scale and ranges of velocity. While the predicted responses are not nearly as noisy as the photogrammetric responses, the curves are in excellent agreement with the overall shape, magnitude, and duration of the test responses.

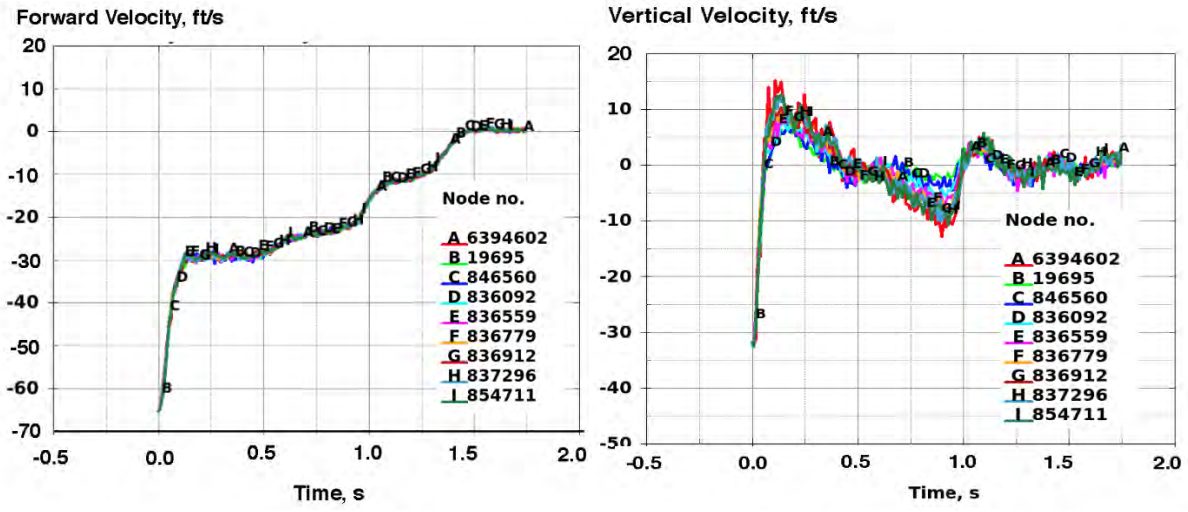

(a)Forward velocity responses. (b) Vertical velocity comparisons.

Figure 15. Analytical predictions of forward and vertical velocities for comparisons with data shown in Figure 14.

As a final kinematic assessment, a comparison of the slide out distance is made, which is the distance from initial impact of the aircraft to its resting position. In this case, a measurement was made between the tip of the nose of the aircraft to the rigid wall, as shown in Figure 16. The same measurement was made for the simulation. The results are shown in Table 2. Based on these data and the previous comparison of velocity responses, the model has matched the kinematic behavior of the test article very well.

Figure 16. Measured distance between the aircraft nose and the rigid wall.

Table 2. Comparison of Distance Between the Nose Tip and the Rigid Wall

Parameter	Distance
Post-test measurement	21.5-ft
Model prediction	21.2-ft
Percentage difference	1.39%

5.3 Structural Acceleration Comparisons

The next category of test-analysis comparisons is structural acceleration results for accelerometers located at the base of the seats and at the airframe/floor intersections. In addition, test-analysis comparisons are shown for the nose cone bulkhead, the port and starboard engine nacelles, and the tail. Please note that both test and predicted acceleration responses were filtered using a 60-Hz low-pass Butterworth filter.

5.3.1 Seat Base Test-Analysis Comparisons

The first test-analysis comparison is for vertical and forward acceleration responses of the pilot seat, as shown in Figure 17. In general, the level of comparison is very good. For this location, the acceleration traces were integrated to generate velocity time histories, which are plotted in Figure 18. The predicted vertical velocity response is nearly an exact match to the test, whereas the forward velocity response indicates that the test removes velocity slightly more quickly than the model, following the initial knee in the curves. Note that the output at this location in the model was generated in the global coordinate system, thus permitting the acceleration to be integrated. All

remaining predicted acceleration responses that are presented in this paper were output using a local coordinate system that was assigned to the node at which output was obtained. Thus, nodal data were generated and output in a local coordinate system. Since the local coordinate system can move with the node, it is not an inertial system. Thus, acceleration traces cannot be integrated to obtain velocity responses.

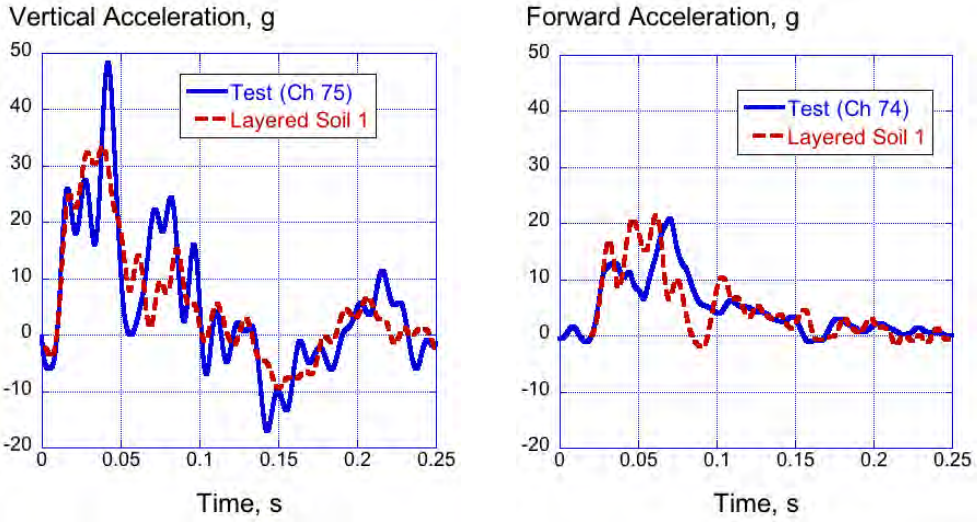

(a)Vertical acceleration responses. (b) Forward acceleration responses.

Figure 17. Pilot seat vertical and forward acceleration comparisons.

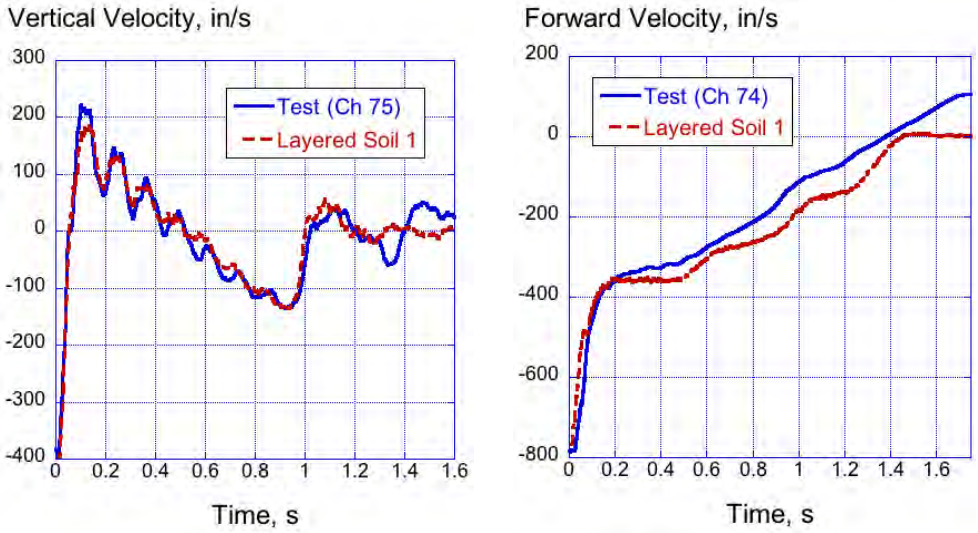

(a)Vertical velocity responses. (b) Forward velocity responses.

Figure 18. Pilot seat vertical and forward velocity comparisons.

The next location for test-analysis comparison is the seat at Row 1 on the Starboard side of the aircraft (see Figure 10 for seat location). Both vertical and forward accelerations are compared in Figure 19. Please note that there was no seat at Row 1 on the Port side due to the presence of the door. Overall, the level of comparison for these two plots is reasonably good. For the vertical acceleration responses, the test data exhibits higher peak oscillations towards the beginning of impact, which is not captured by the model.

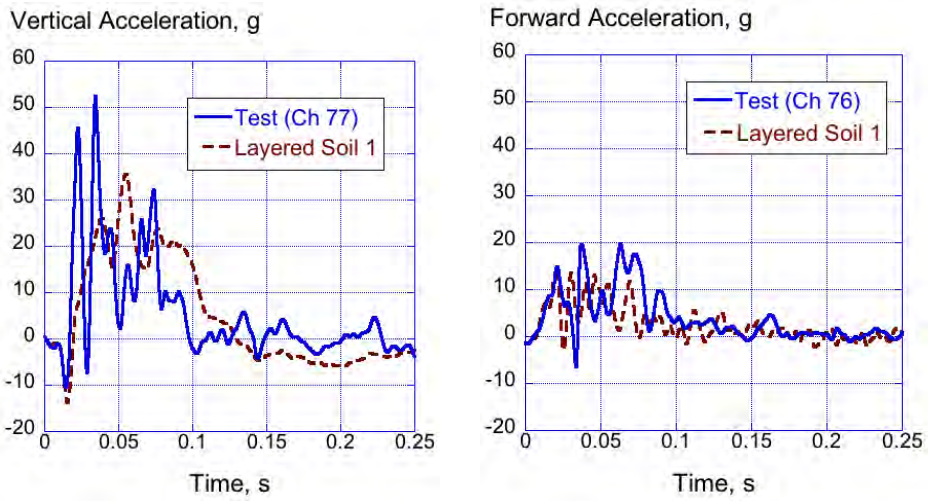

(a)Vertical acceleration responses. (b) Forward acceleration responses.

Figure 19. Starboard Seat Row 1 vertical and forward acceleration comparisons.

The next location for test-analysis comparisons is the seat base at Row 2, which is located in the forward cabin (see Figure 10). The vertical and forward acceleration responses for the starboard and port sides are shown in Figures 20 and 21, respectively. In general, the model does a good job of predicting the overall shape and duration of the responses at this location; however, both predicted vertical acceleration curves over predict the magnitude of the test curves.

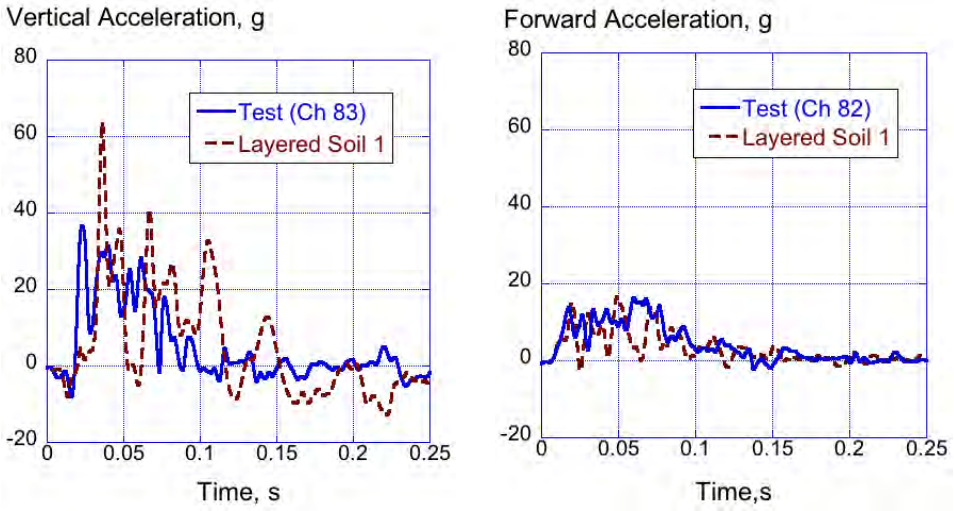

(a)Vertical acceleration responses. (b) Forward acceleration responses.

Figure 20. Row 2 starboard seat vertical and forward acceleration comparisons.

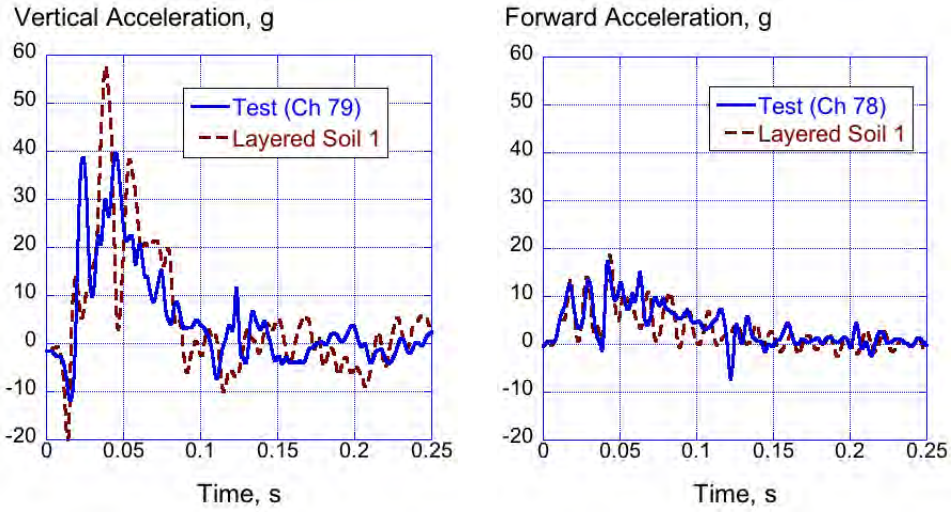

(a)Vertical acceleration responses. (b) Forward acceleration responses.

Figure 21. Row 2 seat port vertical and forward acceleration comparisons.

The next location for test-analysis comparisons is Row 3 (see Figure 10). A plot of vertical acceleration for Row 3 on the starboard side of the airframe is shown in Figure 22. The test response is highly oscillatory, whereas the predicted response in Figure 22 has less noise. Both responses have a similar peak acceleration of 45- to 47-g. Note that the forward acceleration data channel was over-ranged and consequently this comparison is not shown. Plots of forward and vertical acceleration on the port side of the aircraft are shown in Figure 23 for Row 3. In general, the model does a good job of predicting the overall magnitude, shape, and duration of the test acceleration. However, the test

forward response, shown in Figure 23(b), agrees well for the first 0.05-seconds, then shows two large acceleration spikes of higher magnitude than the predicted response.

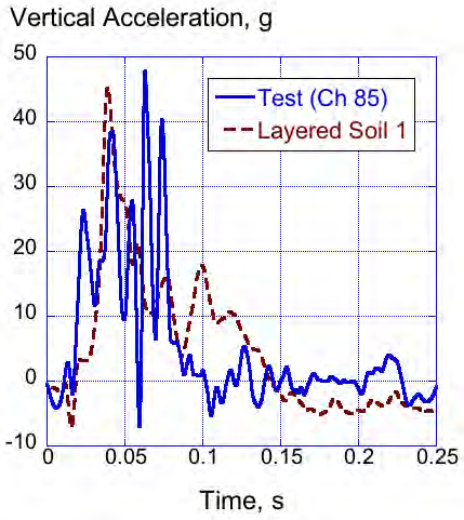

Figure 22. Test-analysis plot of vertical acceleration at starboard Row 3.

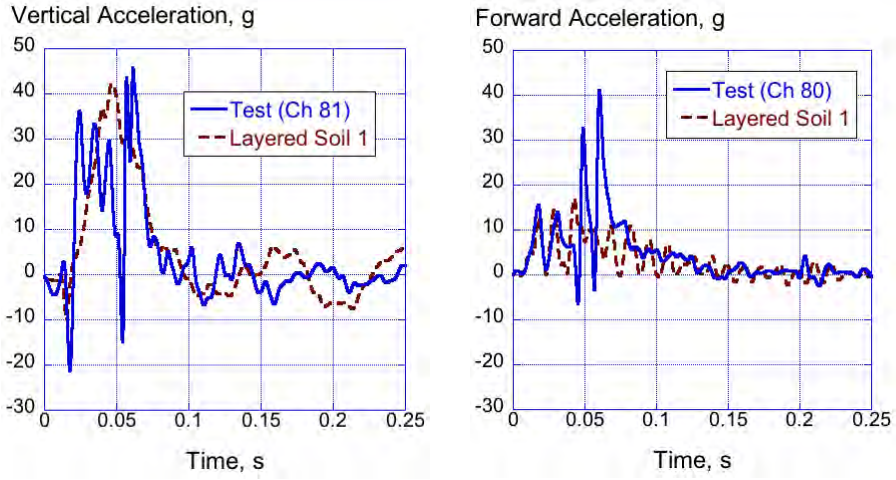

(a)Vertical acceleration responses. (b) Forward acceleration responses.

Figure 23. Row 3 port seat vertical and forward acceleration comparisons.

The next location for test-analysis comparisons is Row 5, which is located in the mid-cabin region of the aircraft, just forward of the wing (see Figure 10). Plots of vertical and forward acceleration are shown in Figure 24 for the starboard seat in Row 5. The overall shape and magnitude of the vertical acceleration is well predicted by the model; however, the test forward acceleration response has a higher magnitude response than the model. Likewise, plots of vertical and forward acceleration are shown in Figure 25 for the port seat in Row 5.

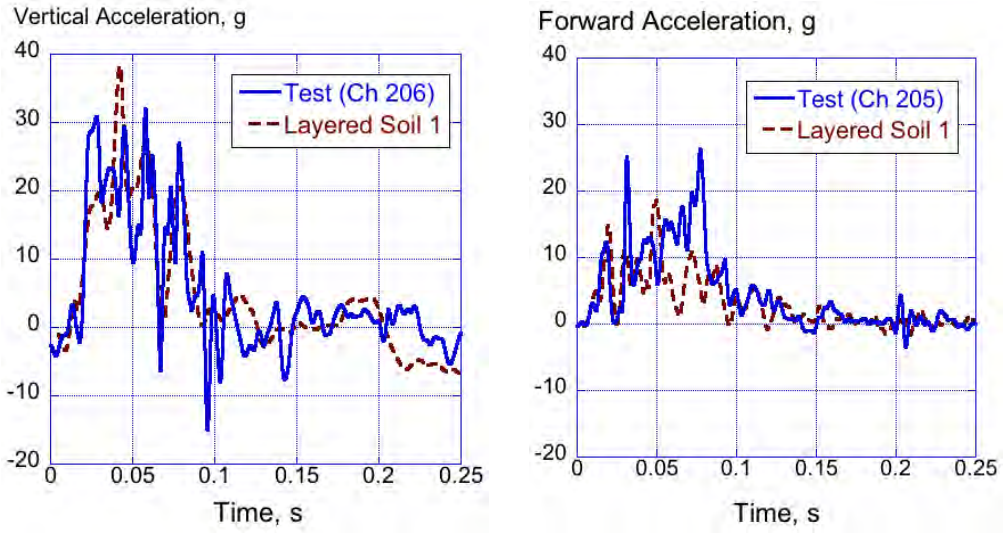

(a)Vertical responses. (b) Forward responses.

Figure 24. Row 5 starboard seat vertical and forward acceleration comparisons.

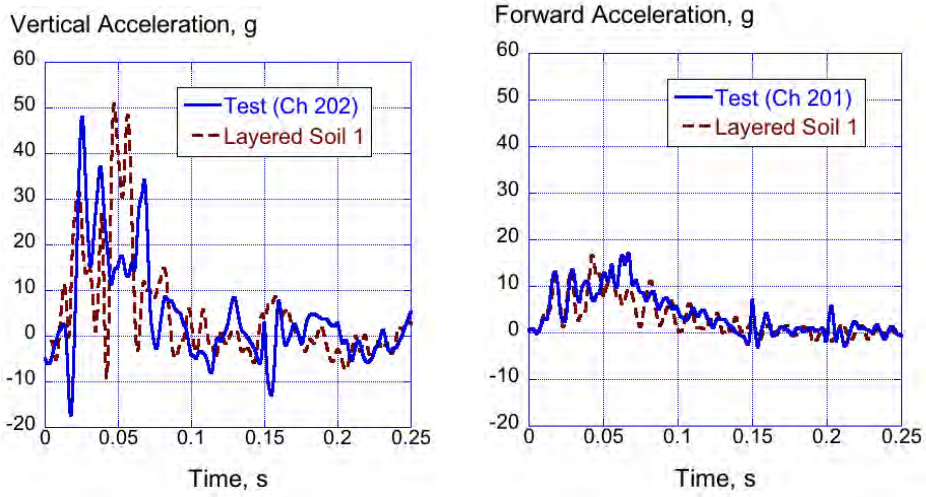

(a)Vertical responses. (b) Forward responses.

Figure 25. Row 5 port seat vertical and forward acceleration comparisons.

The next seat base comparison is for Row 6, which is located in the mid-cabin over the wing (see Figure 10). Only the forward acceleration responses for the starboard side are shown in Figure 26, due to over-ranging of the vertical accelerometer. The test response in Figure 26 exhibits a large spike in acceleration at approximately 0.04-seconds, ranging from 35- to -10-g. Both vertical and forward acceleration comparisons are plotted in Figure 27 for the port row 6 seat. The predicted responses are reasonably close in magnitude, shape, and duration of the test responses. However, it is interesting to note that both test forward acceleration responses, depicted in Figure 26 and Figure

27(b), show a large spike in the acceleration response at approximately 0.05-s. The spikes are not seen in the predicted data, nor in the test vertical acceleration response. It is assumed that the spikes in acceleration may be attributed to failure of the port side wing.

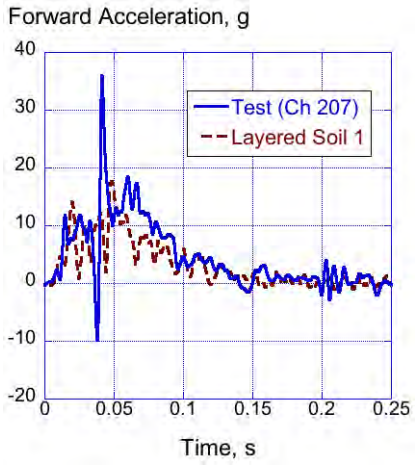

Figure 26. Row 6 starboard seat forward acceleration comparisons.

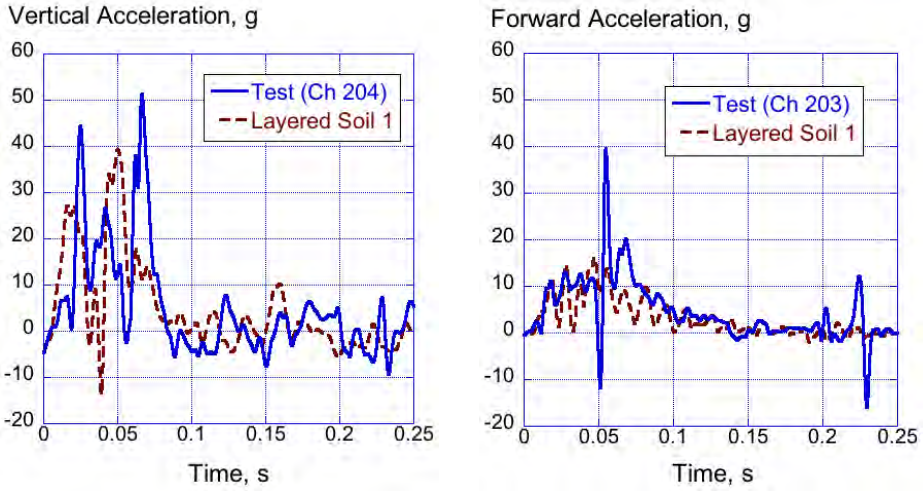

(a)Vertical acceleration responses. (b) Forward acceleration responses.

Figure 27. Row 6 port seat vertical and forward acceleration comparisons.

The next location for seat base comparisons is the starboard seat at Row 8. Both vertical and forward test-analysis acceleration plots are shown in Figure 28. It is interesting to note that the vertical acceleration test response contains high frequency oscillations, which are matched in the analytical predictions. Note that Row 8 is located just behind the wing.

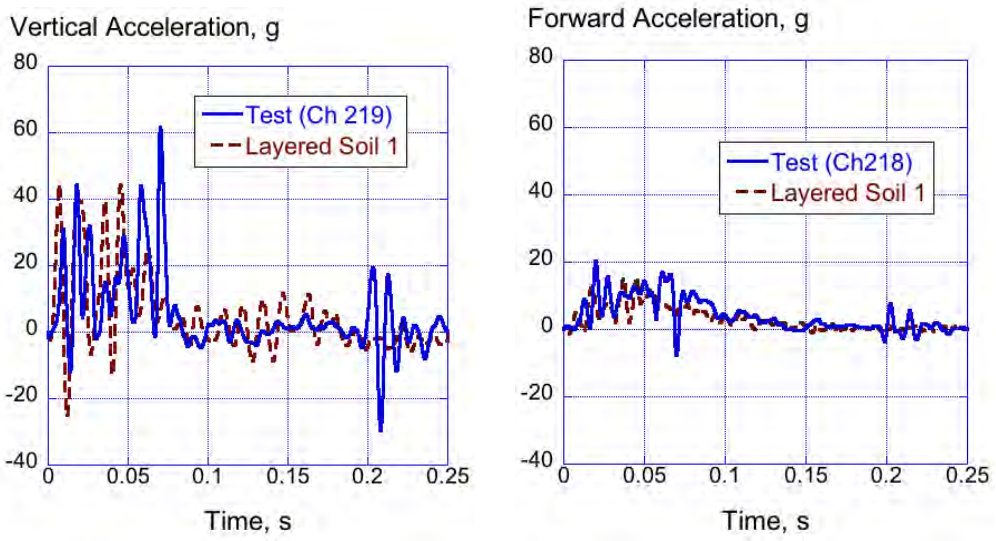

(a)Vertical acceleration responses. (b) Forward acceleration responses.

Figure 28. Row 8 starboard seat vertical and forward acceleration comparisons.

The next location for seat base test-analysis comparisons is Row 9, which is near the rear-cabin of the fuselage. Plots of test-analysis vertical and forward accelerations are plotted in Figure 29 for the starboard seat at Row 9. The forward acceleration test response is dominated by a large spike, which occurs just after 0.1-s. Two additional spikes occur after 0.15-s, which are smaller in magnitude. Test-analysis vertical and forward acceleration responses are shown in Figure 30 for the port seat at Row 9. At this location, both the vertical and forward test acceleration responses exhibit a spike at 0.2-seconds, which is not seen in the predicted responses.

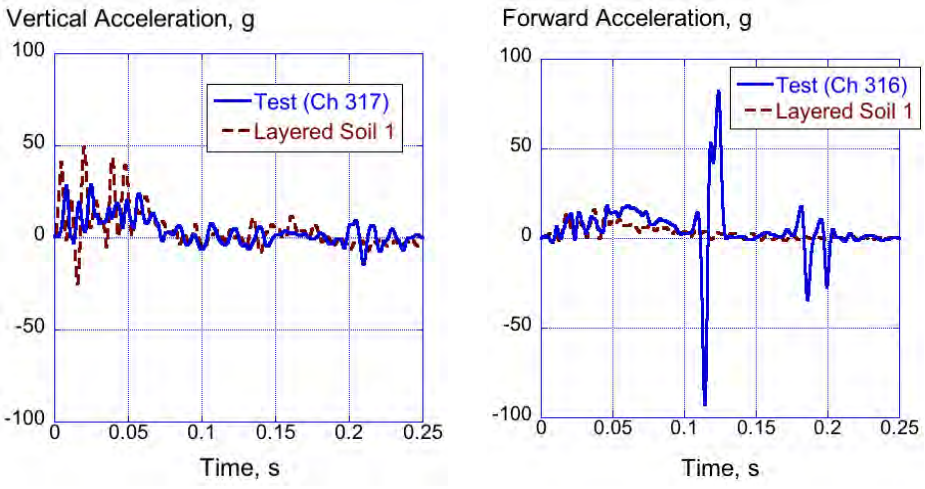

(a)Vertical acceleration responses. (b) Forward acceleration responses.

Figure 29. Row 9 starboard side seat vertical and forward acceleration comparisons.

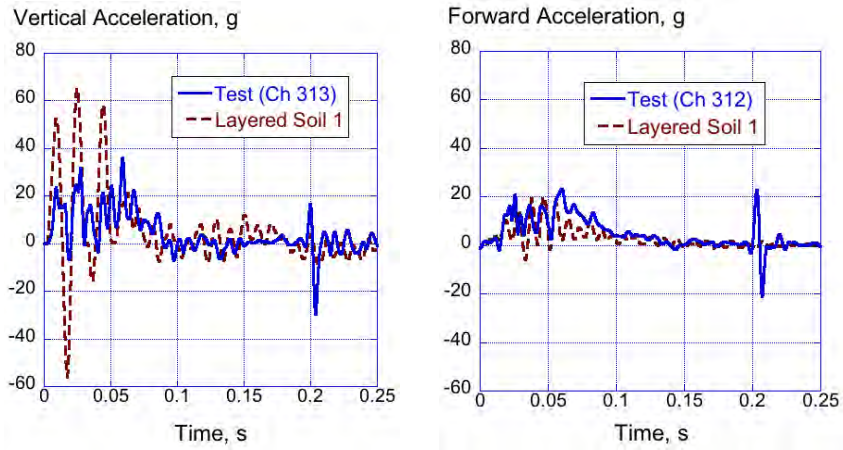

(a)Vertical acceleration responses. (b) Forward acceleration responses.

Figure 30. Row 9 starboard side seat vertical and forward acceleration comparisons.

The next test-analysis comparison is for the port seat at Row 10, which is located in the rear cabin. Plots of vertical and forward acceleration responses are shown in Figure 31 for the port seat. At this location, large spikes are observed in the predicted vertical acceleration response; however, the spike in the test forward acceleration response that previously occurred at approximately 0.2-seconds is gone.

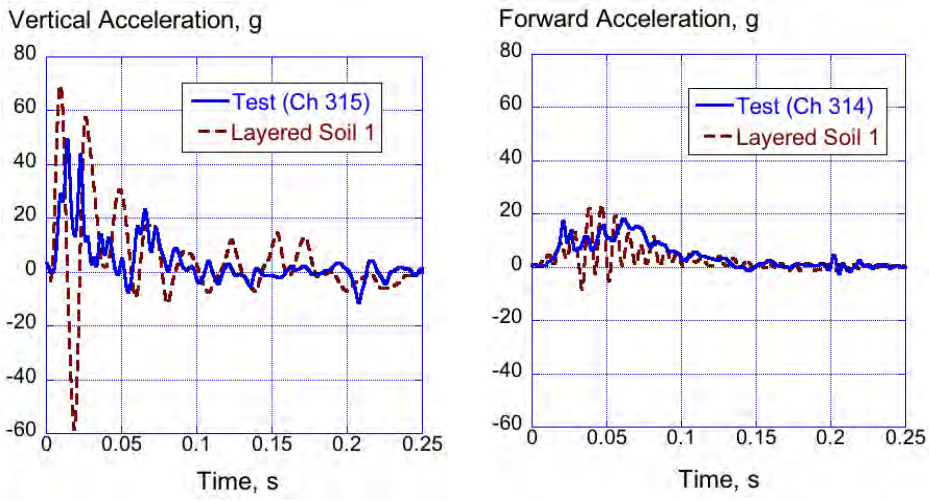

(a)Vertical acceleration responses. (b) Forward acceleration responses.

Figure 31. Row 10 port seat vertical and forward acceleration comparisons.

As a final seat base comparison, the forward acceleration response of the starboard seat at Row 12 is plotted in Figure 32. Row 12 is located in the very rear of the aircraft, as indicated in Figure 10. The

test vertical acceleration response contains high frequency oscillations, including an acceleration spike at approximately 0.025seconds that ranges from 32- to -14-g. The predicted response exhibits oscillations in the acceleration, matching the test behavior. Note that the vertical accelerometer at Row 12 was over ranged.

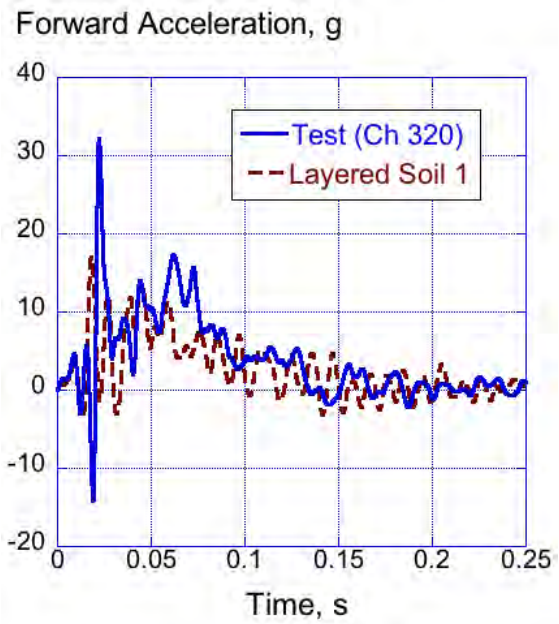

Figure 32. Starboard seat at Row12 forward test-analysis acceleration comparison.

5.3.2 Test-Analysis Comparisons at the Airframe/Floor Intersections

The next area of test-analysis comparison is for the airframe/floor intersection accelerometers. A schematic drawing the aircraft depicting the location of these accelerometers in shown in Figure 7. Also, a photograph showing one of the airframe/floor accelerometers is shown in Figure 8(a). The first comparison is for the port frame vertical and forward accelerometers at FS 2200, as shown in Figure 33. The vertical and forward acceleration comparisons are plotted in Figure 34 for the starboard airframe at FS 3050. At both locations, the predicted responses generally match the shape, magnitude, and duration of the test responses.

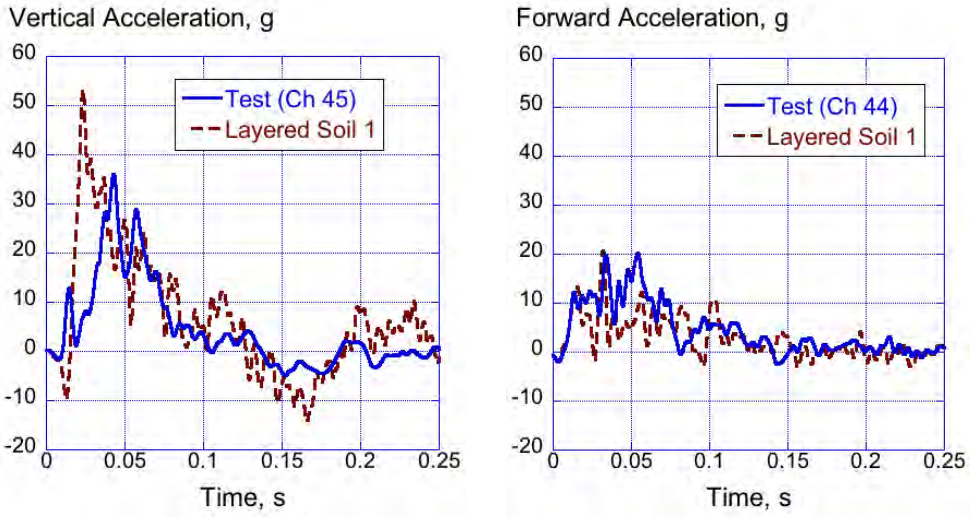

(a)Vertical acceleration responses. (b) Forward acceleration responses.

Figure 33. Port acceleration comparisons at the airframe/floor intersection at FS 2200.

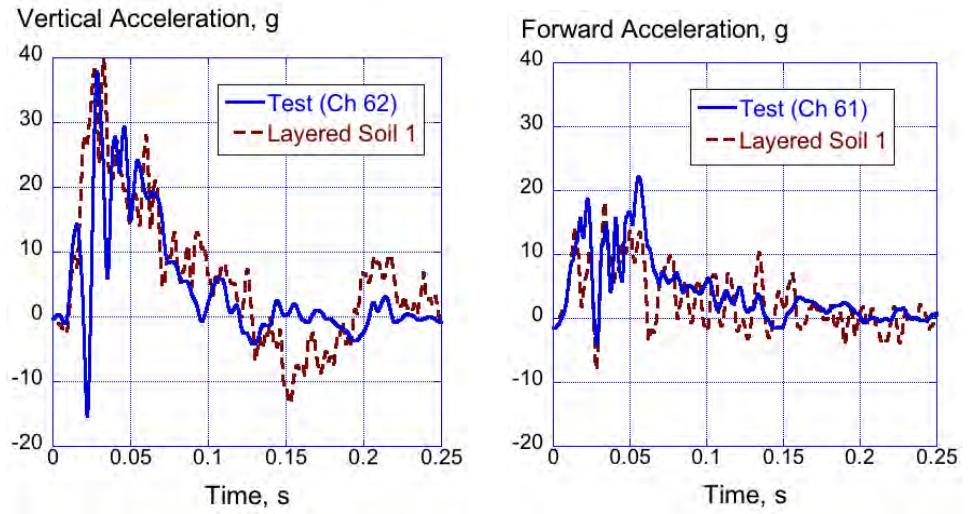

(a)Vertical acceleration responses. (b) Forward acceleration responses.

Figure 34. Starboard acceleration comparisons at the airframe/floor intersection at FS 3050.

The next locations for test-analysis comparisons are the port airframe at FS 6805 (Figure 35) and the starboard airframe at FS 6305 (Figure 36). At both locations, the predicted vertical acceleration responses contain high frequency oscillations, which have higher magnitude peaks than the test responses. The opposite is true for the forward acceleration responses.

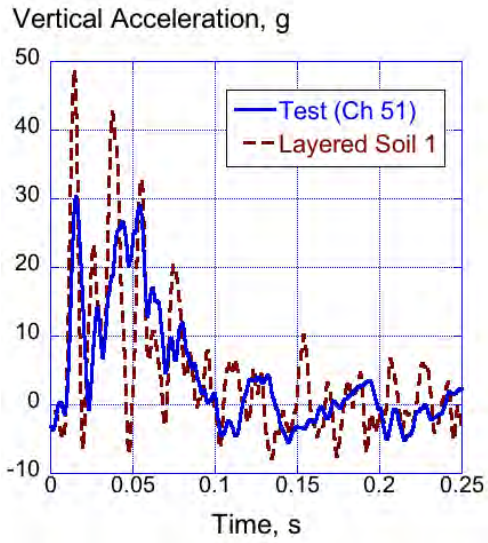

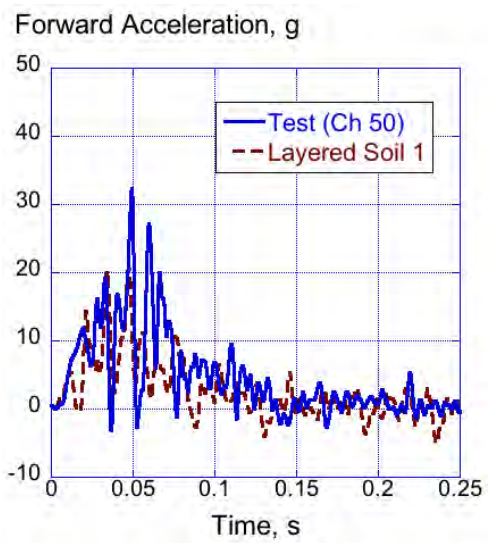

(a)Vertical acceleration responses. (b) Forward acceleration responses.

Figure 35. Port acceleration comparisons at the airframe/floor intersection at FS 6805.

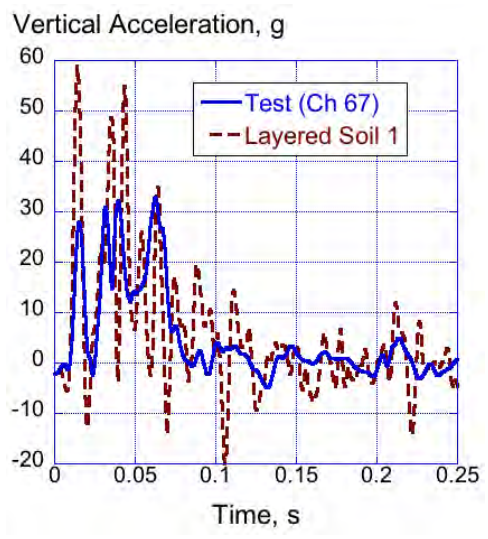

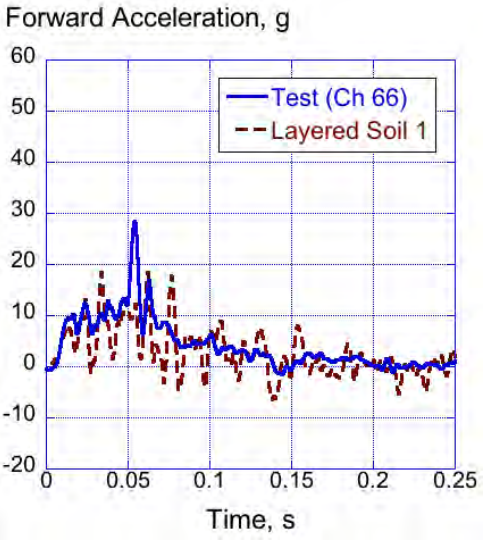

(a)Vertical acceleration responses. (b) Forward acceleration responses.

Figure 36. Starboard acceleration comparisons at the airframe/floor intersection at FS 6305.

The next locations for test-analysis comparisons are the port airframe at FS 7805 (Figure 37) and the starboard airframe at FS 7305 (Figure 38). The test vertical acceleration response on the port side at FS 7805 (Figure 37(a)) appears to flat line after 0.05-seconds, whereas the predicted response exhibits three spikes in acceleration of descending magnitude. Each spike is higher in magnitude than the test. Also, the test forward acceleration response, shown in Figure 37(b) exhibits large spikes in the

acceleration response beginning at 0.05-seconds. These same spikes also appear in the forward test acceleration response of the airframe at FS 7305.

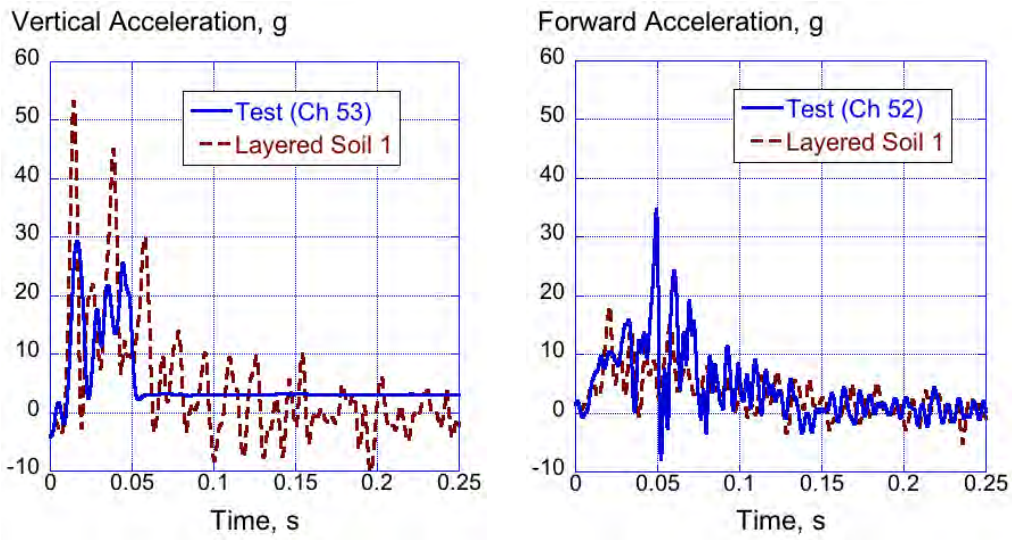

(a)Vertical acceleration responses. (b) Forward acceleration responses.

Figure 37. Port acceleration comparisons at the airframe/floor intersection at FS 7805.

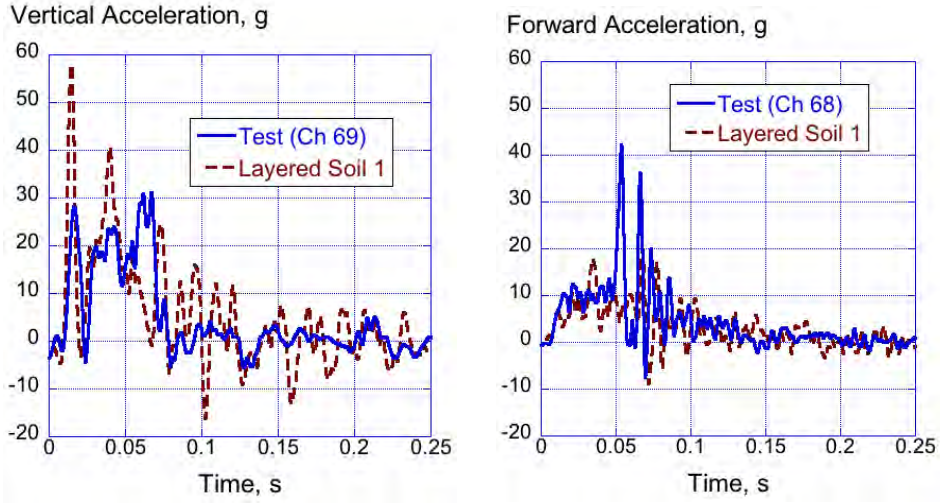

(a)Vertical acceleration responses. (b) Forward acceleration responses.

Figure 38. Starboard acceleration comparisons at the airframe/floor intersection at FS 7305.

The next locations for test-analysis comparisons are the port airframe at FS 8805 (Figure 39) and the starboard airframe at FS 8305 (Figure 40). In general, the model does a reasonably good job of matching the shape, magnitude, and duration of the test responses at both locations. The vertical acceleration responses show better agreement than do the forward responses. Note that the test

forward acceleration response at FS 8305 (see Figure 40(b)) exhibits oscillatory spikes after 0.05-seconds. This behavior is not seen in the predicted response.

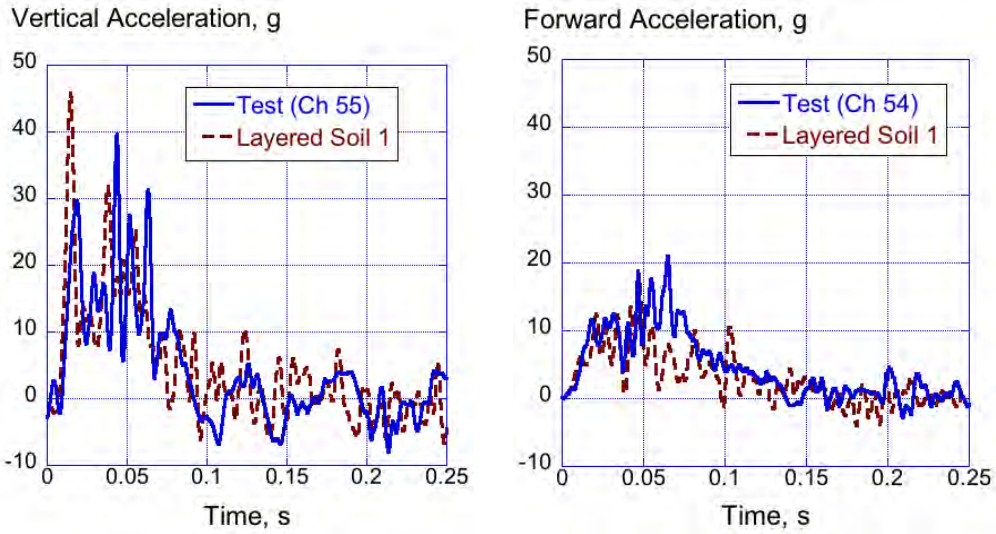

(a)Vertical acceleration responses. (b) Forward acceleration responses.

Figure 39. Port acceleration comparisons at the airframe/floor intersection at FS 8805.

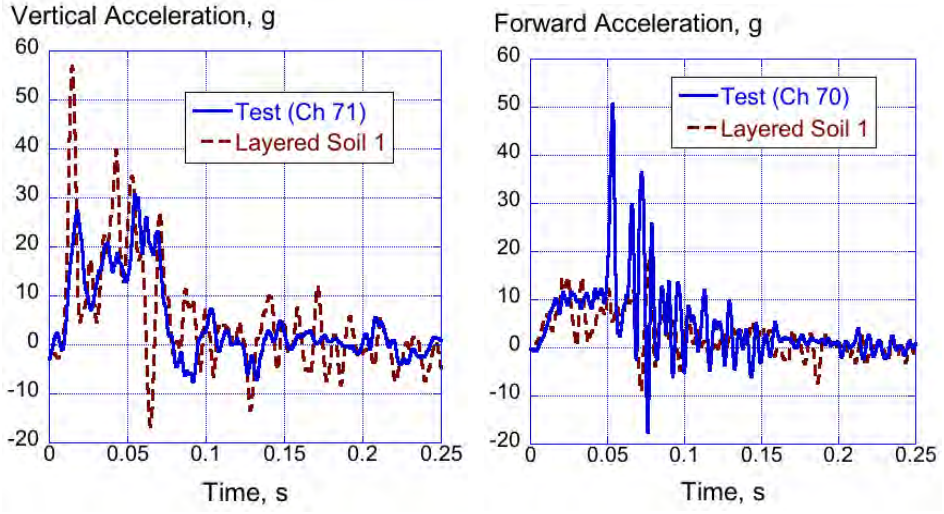

(a)Vertical acceleration responses. (b) Forward acceleration responses.

Figure 40. Starboard acceleration comparisons at the airframe/floor intersection at FS 8305.

The next locations for test-analysis comparisons are the port airframe at FS 9805 (Figure 41) and the starboard airframe at FS 9305 (Figure 42). Both the test and predicted acceleration responses at these two locations appear to have a less noisy response. The reason for this behavior may be that the channel locations are near the rear of the aircraft, where the mass is higher.

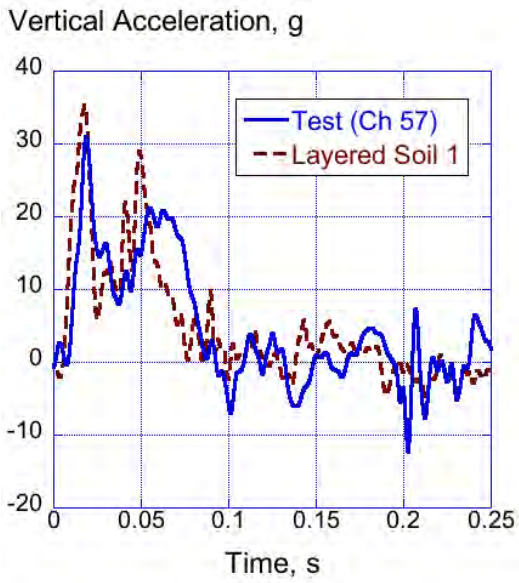

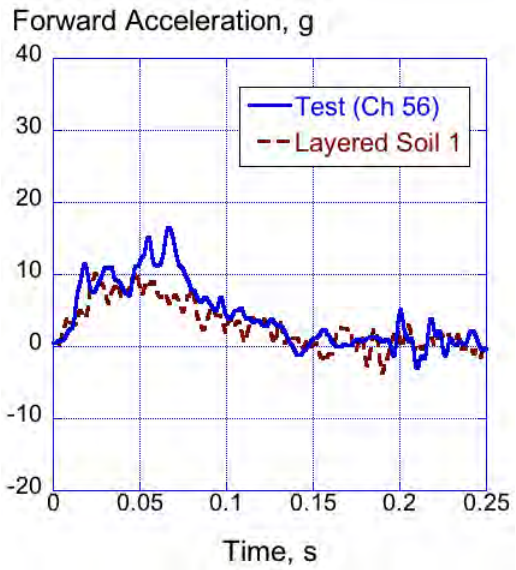

(a)Vertical acceleration responses. (b) Forward acceleration responses.

Figure 41. Port acceleration comparisons at the airframe/floor intersection at FS 9805.

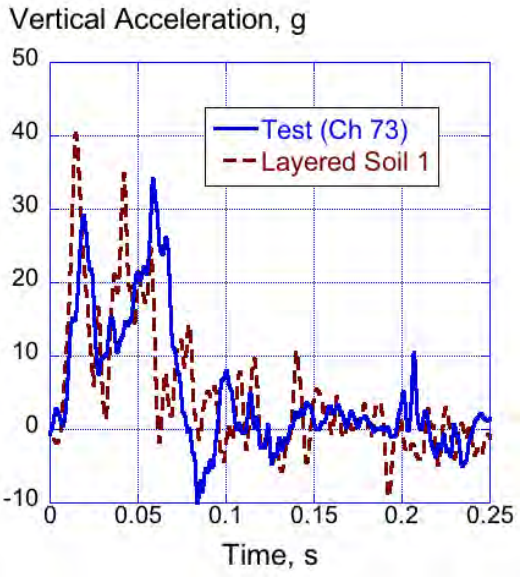

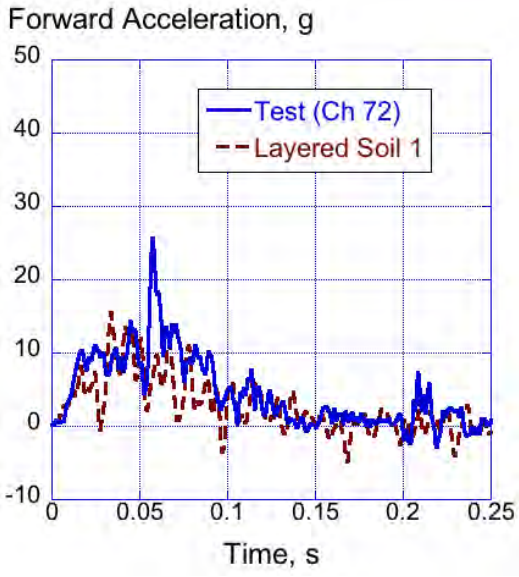

(a)Vertical acceleration responses. (b) Forward acceleration responses.

Figure 42. Starboard acceleration comparisons at the airframe/floor intersection at FS 9305.

The next locations for test-analysis comparisons are the port airframe at FS 10790 (Figure 43) and the starboard airframe at FS 10305 (Figure 44). In general, the model responses match the overall

shape and duration of the test responses, though the magnitudes of the test responses are in some cases over predicted and under predicted in others.

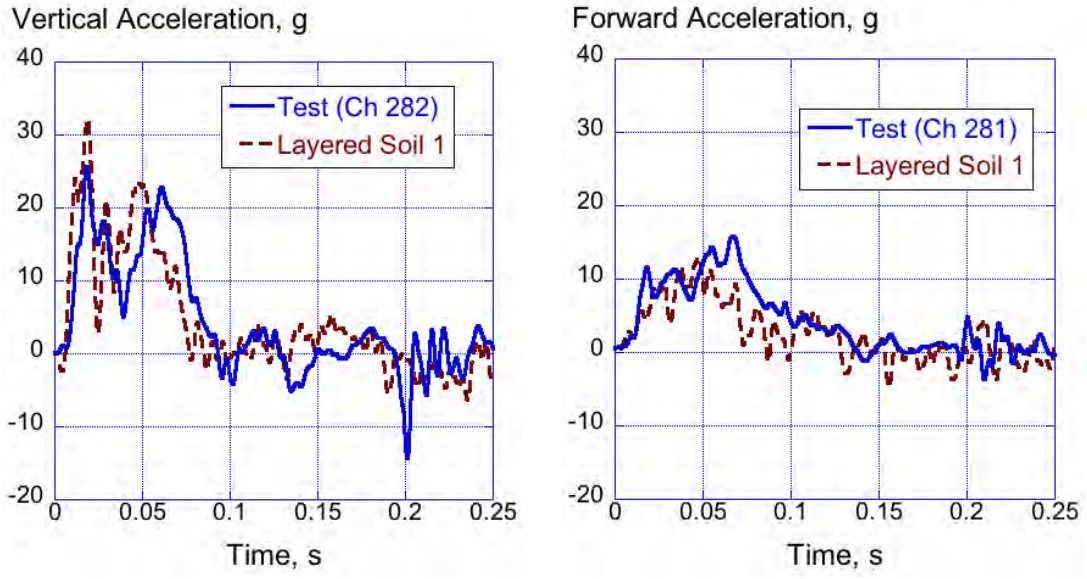

(a)Vertical acceleration responses. (b) Forward acceleration responses.

Figure 43. Port acceleration comparisons at the airframe/floor intersection at FS 10790.

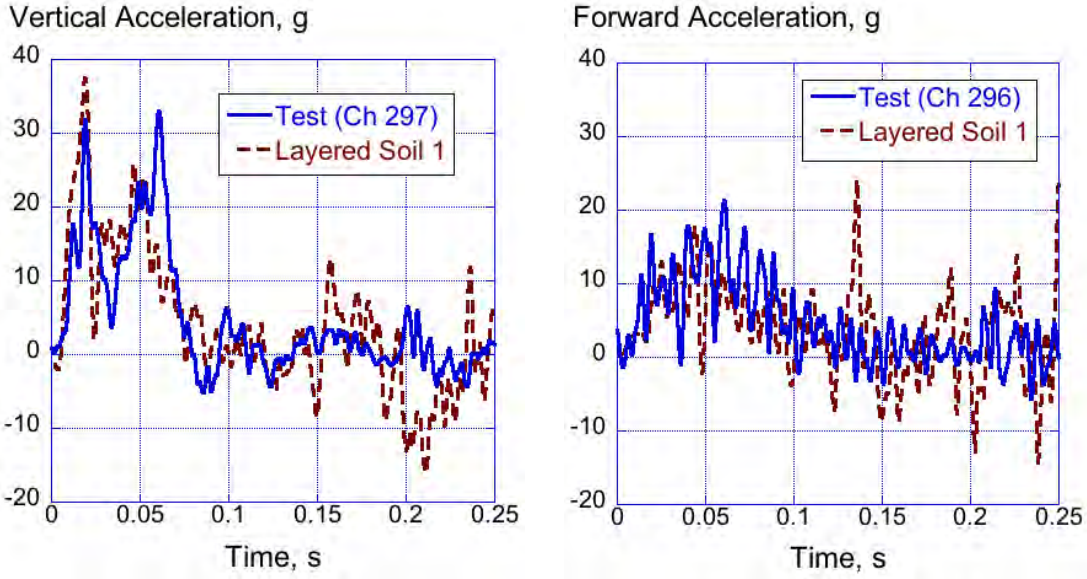

(a)Vertical acceleration responses. (b) Forward acceleration responses.

Figure 44. Starboard acceleration comparisons at the airframe/floor intersection at FS 10305.

The test-analysis comparisons for the airframe/floor interfaces are for the port side at FS 11905 (Figure 45), starboard side at FS 12405 (Figure 46), port side at FS 12875, and the starboard side at FS 13345 (Figure 48). In general, the predicted responses match the overall shape, magnitude, and duration of the test responses. Please note that test-analysis comparisons will be quantified in Section 5.6.

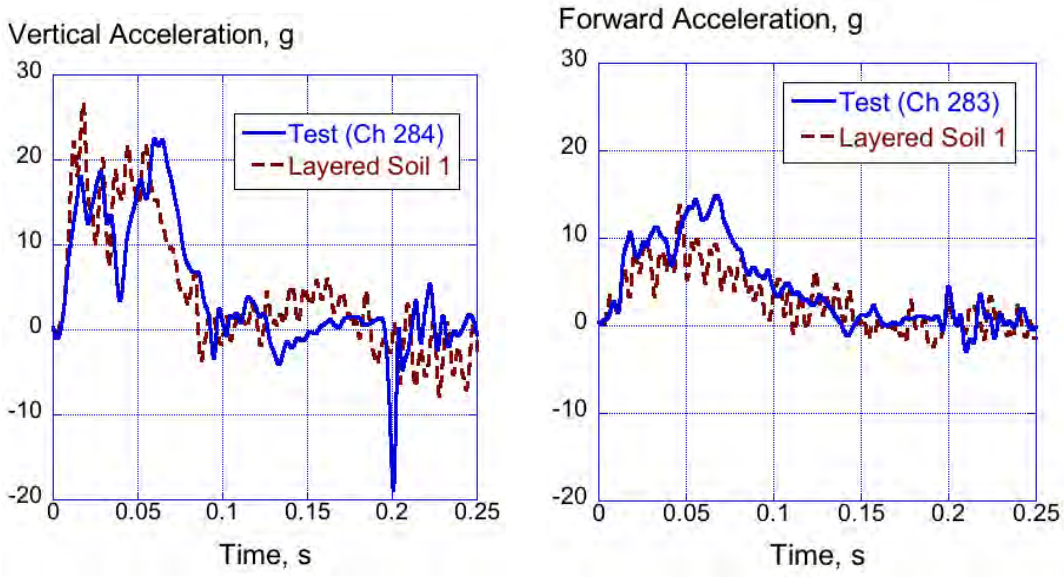

(a)Vertical acceleration responses. (b) Forward acceleration responses.

Figure 45. Port acceleration comparisons at the airframe/floor intersection at FS 11905.

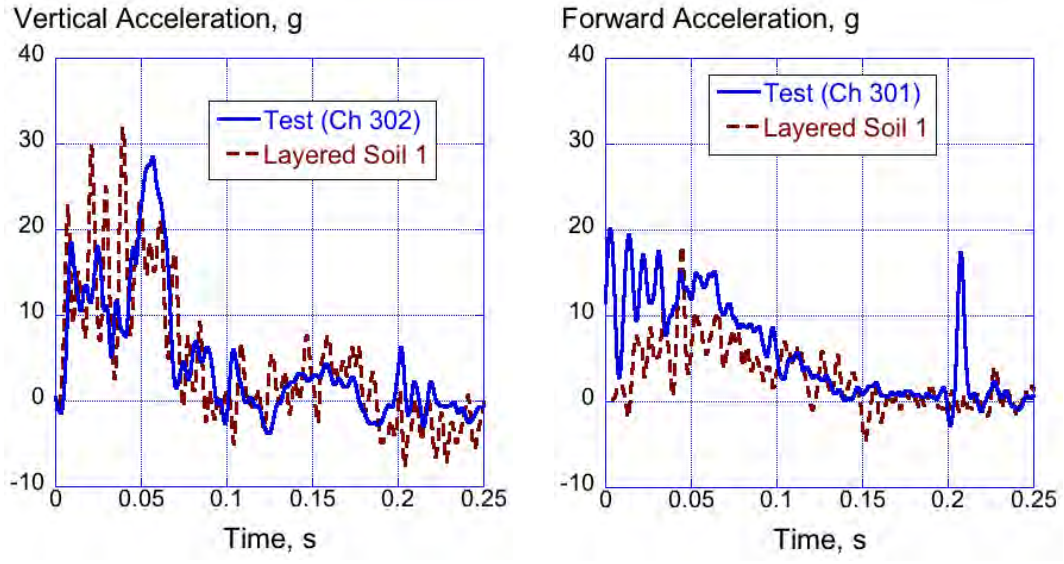

(a)Vertical acceleration responses. (b) Forward acceleration responses.

Figure 46. Starboard acceleration comparisons at the airframe/floor intersection at FS 12405.

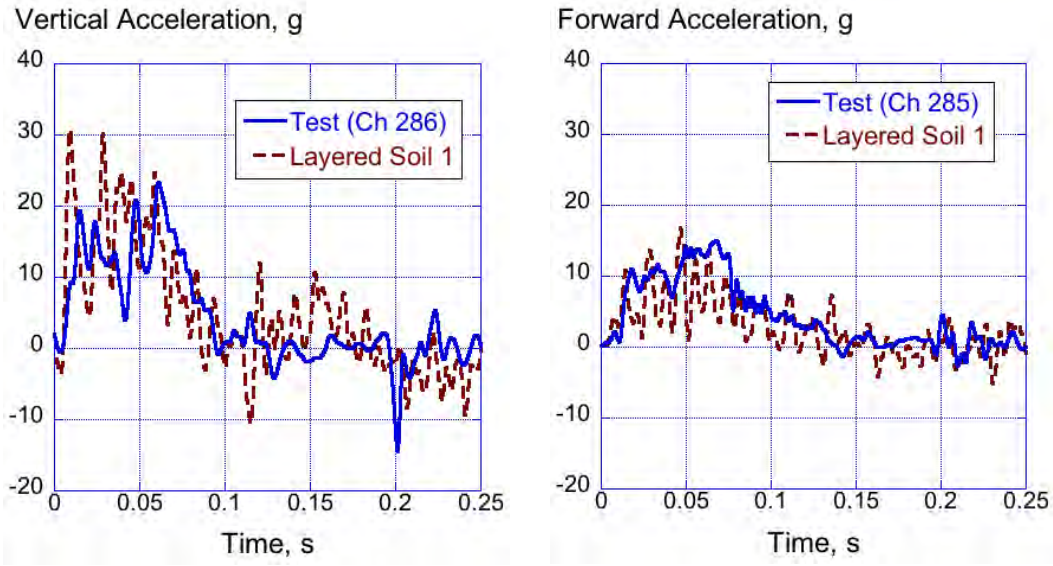

(a)Vertical acceleration responses. (b) Forward acceleration responses.

Figure 47. Port acceleration comparisons at the airframe/floor intersection at FS 12875.

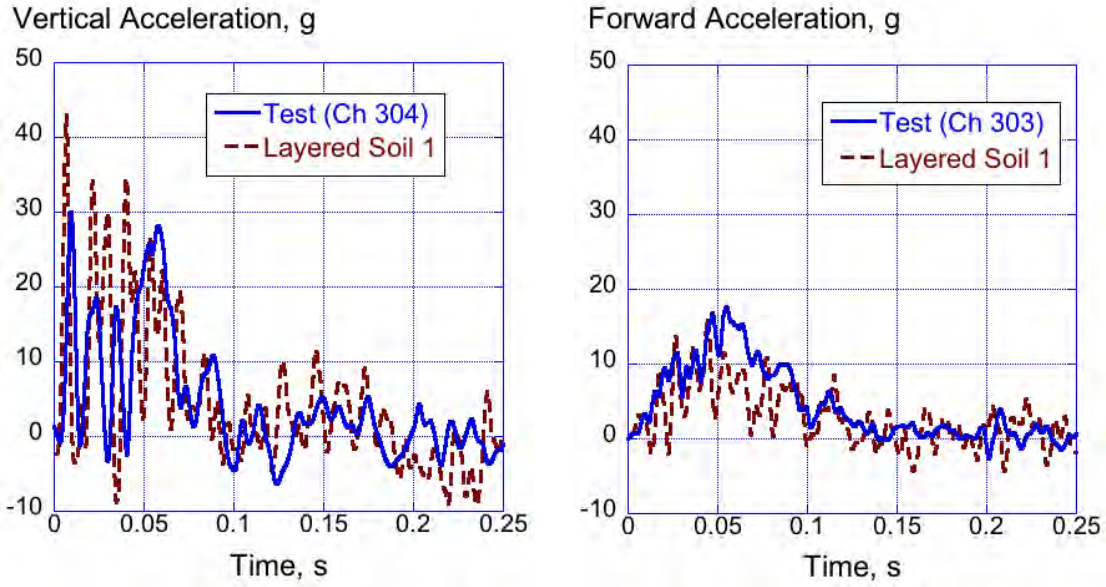

(a)Vertical acceleration responses. (b) Forward acceleration responses.

Figure 48. Starboard acceleration comparisons at the airframe/floor intersection at FS 13345.

5.3.3 Test-Analysis Comparisons of Discrete Airframe Locations

A final test-analysis comparison is presented in this section for four locations on the aircraft: the nose cone bulkhead, the port and starboard engine nacelles, and the tail. Test-analysis forward and vertical acceleration responses are shown in Figure 49 for the nose cone, along with a depiction of the location

of the node where the accelerometer was located. The model generally over predicted the magnitude of the test vertical acceleration response; however, the overall shape and pulse duration were well matched. In the forward acceleration plot, the test response contained a large spike in acceleration at 0.075-seconds, that was not observed in the predicted response.

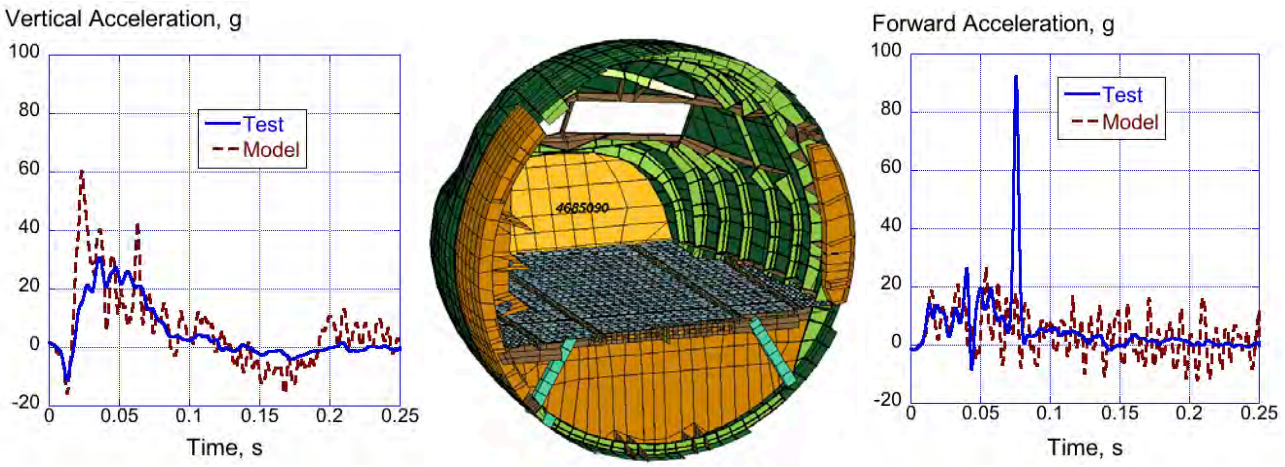

Figure 49. Test-analysis comparisons for the nose cone bulkhead location.

Next, the forward and vertical acceleration responses are shown in Figure 50 for the port and starboard engine nacelle locations. In general, the model does a reasonably good job of matching the test responses at both locations.

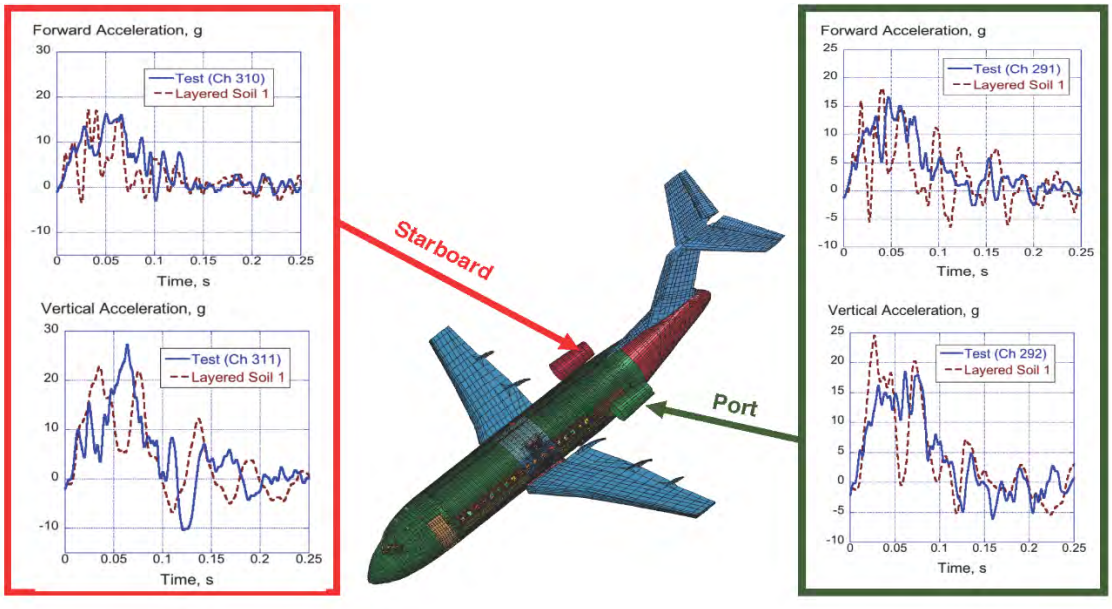

Figure 50. Test-analysis acceleration comparisons for the port and starboard engine nacelles.

Finally, the test-analysis comparisons for the forward and vertical acceleration responses of the tail are depicted in Figure 51. The predicted responses are generally a good match to the test data. The vertical test response exhibits high frequency oscillations after 0.1-seconds, which are not observed in the predicted response.

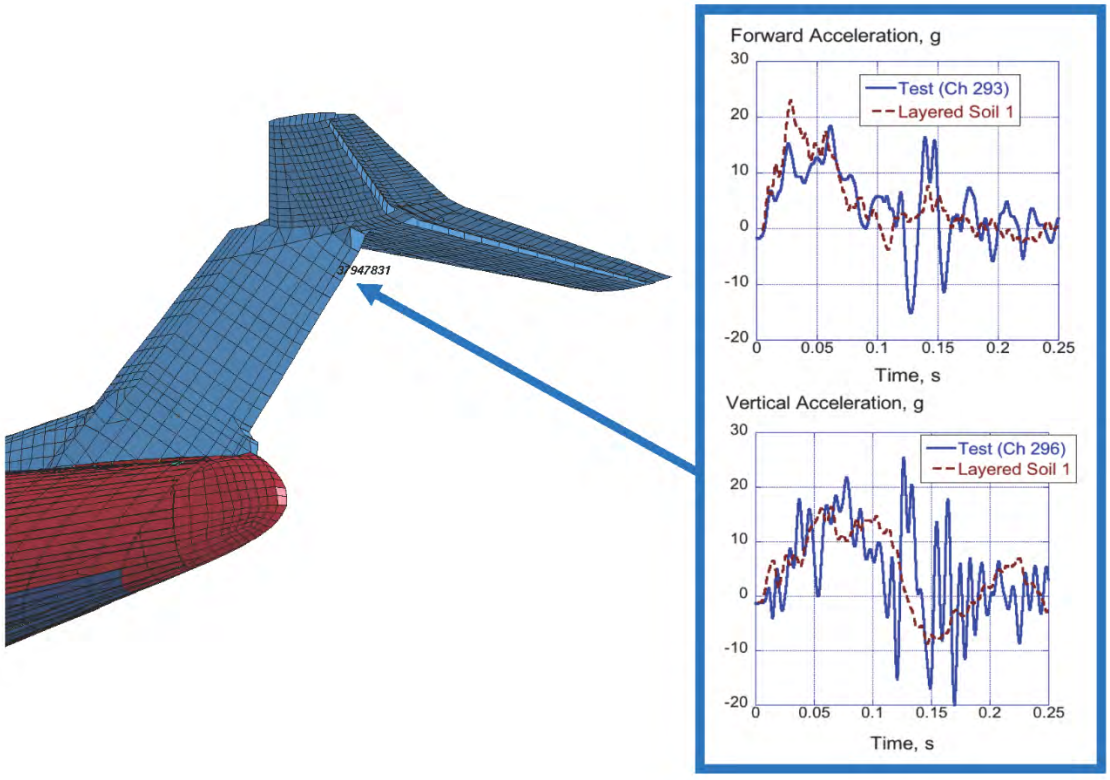

Figure 51. Test-analysis acceleration comparisons for the tail section.

5.4 Airframe Deformation and Failure

Viewing the aircraft externally following the test, it is difficult to observe much damage to the test article. The most evident damage is wrinkling and buckling of the exterior skin, as shown in Figure 52(a). In addition, the port side wing broke away from the aircraft, as depicted in Figure 52(b). The wing separation was caused by failure of several bolts used to attach the wing to the airframe. Note that in the model the wing was rigidly fixed to the frame, and thus did not predict the wing attachment failure. Following the test, the aircraft was raised and moved away from the soil surface using the lifting hardware located at the wing attachment. Substantial damage was revealed in the form of crushing and flattening of the lower cargo subfloor, tearing of metal airframe structures near the lower wing-box section, and skin wrinkling, as shown in Figures 53 and 54. Predicted damage to the model is also shown, which corresponds well with the physical damage.

(a)Photo of skin wrinkling. (b) Photo of port wing separation.

Figure 52. Depictions of damage to the aircraft.

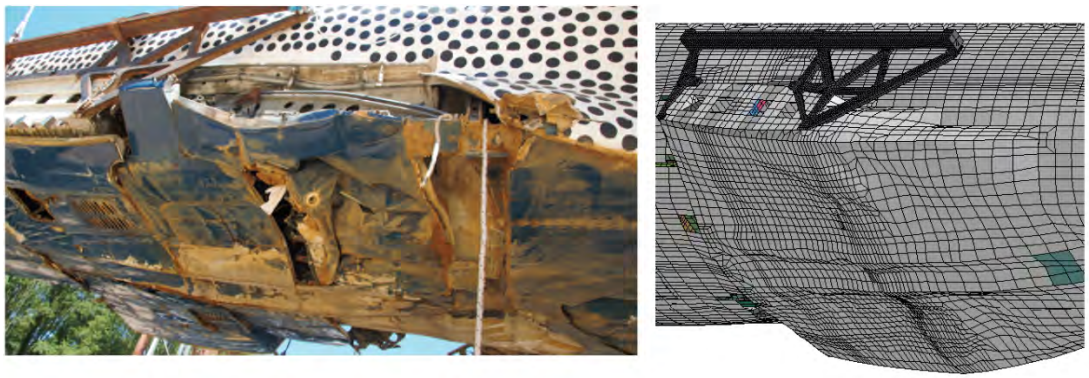

(a)Photograph of airframe damage. (b) Model damage.

Figure 53. Damage to the underbelly of the aircraft, forward of the wing-box section.

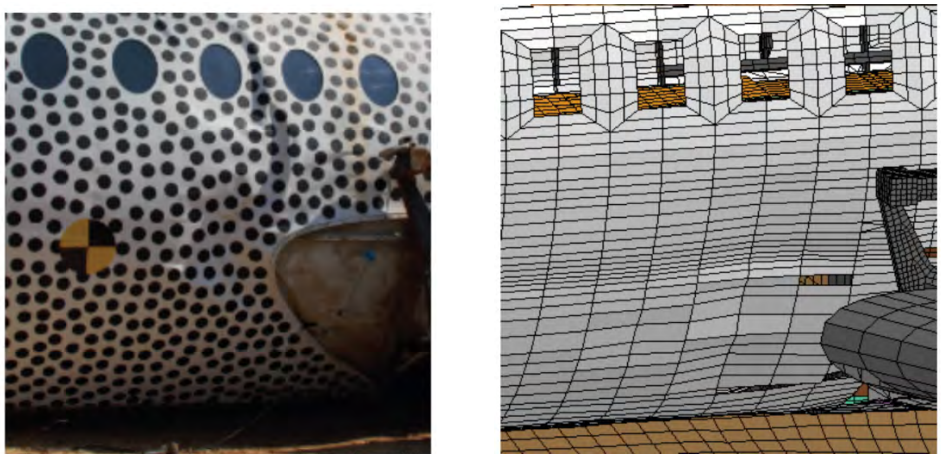

(a)Photo depicting wrinkling of the outer skin. (b) Model damage.

Figure 54. Damage to the fuselage skin.

5.5 Quantitative Test-Analysis Results

Several commercial software codes are available for predicting the transient dynamic response of vehicle structures subjected to impact. Some of these programs are: ABAQUS Explicit [38], PAM-CRASH [39], RADIOSS [40], and LS-DYNA [30-32]. To maximize the use of these codes and to build confidence in their application, the validity of their predictive capabilities needs to be assessed quantitatively. Model validation is the process of comparing model outputs with test measurements in order to assess the validity of the model. One of the critical tasks to achieve quantitative assessment of models is to develop a validation metric that can quantify the discrepancy between time history responses from a physical test and simulation results from a dynamic simulation. Note that developing quantitative model validation methods has attracted considerable interest, with many prior methods documented in References 41-46.

For the ISO/TR-16250 curve comparison methodology [24], four state-of-the-art objective rating metrics are investigated, and they are: CORrelation and Analysis (CORA) metric [47, 48]**;** Error Assessment of Response Time Histories (EARTH) metric [49, 50]; model reliability metric [51-53]; and Bayesian confidence metric [54-56]. Further enhancements of the CORA corridor rating and the development of an Enhanced Error Assessment of Response Time Histories (EEARTH) metric were incorporated to improve the robustness of these metrics. A new combined objective rating, R, metric is developed to standardize the calculation of the correlation between two time-history curves. A Matlab computer program was obtained that performs the test-analysis correlation and outputs the results in five categories: overall ISO objective rating (R), EEARTH magnitude, EEARTH slope, EEARTH phase, and CORA. The objective ISO rating score ranges from 0 to 1 and the higher the score, the better the correlation between the two time-history curves. In the ISO/TR 16250, a grade is assigned based on the objective rating score, R, as shown in Table 3. The ISO TR/16250 objective rating (R) metric was applied to all structural test-analysis responses presented in this paper. The results are listed in Table 4.

Table 3. Sliding Scale of the Overall ISO Rating.

Rank	Grade	Rating, R	Description
1	Excellent	$R > 0.94$	Almost perfect characteristics of the reference signal
2	Good	$0.8 < R \geq 0.94$	Reasonably good characteristics of the reference signal are captured, but noticeable differences between the two curves
3	Fair	$0.58 < R \geq 0.8$	Basic Characteristics of the reference signal are captured; but there are significant differences between curves
4	Poor	$R \leq 0.58$	Almost no correlation between the two curves

Based on the overall ISO ratings listed in Table 3, none of the test-analysis curves exhibited excellent correlation and only one channel (pilot seat vertical velocity) exhibited good correlation. Forty-six

of sixty-seven channels demonstrated fair agreement, while the remaining channels had poor agreement. It should be noted that the ISO TR/16250 document contains several example cases including one involving a sled test with a seated and restrained dummy occupant. Values of the overall ISO rating ranged from 0.906 to 0.456 for the 5th percentile Hybrid III female dummy. Of the initial 11 responses evaluated, three channels showed good agreement, while the remainder showed fair to poor agreement. Several NASA Engineering and Safety Center (NESC) studies have found the ISO/TR 16250 rating system to be too harsh and, instead, generally use a value of 0.5 to determine if the correlation is adequate or not [57]. If 0.5 is applied as the delimiter for this correlation study, then 63 of 67 test-analysis responses, shown in Table 4, would be deemed adequate.

Table 4. ISO 16250 Objective Rating Metrics

No.	Location	ISO Rating, R	EEARTH Magnitude	EEARTH Slope	EEARTH Phase	CORA
Test-Analysis Comparisons of Seat Base Locations						
1	Pilot Seat, Ax	0.59	0.44784	0	0.58723	0.669
2	Pilot Seat, Az	0.74	0.46874	0.52197	0.58723	0.547
3	Pilot Seat, Vx	0.7547	0.94169	0.52414	0.35	0.937
4	Pilot Seat, Vz	0.9227	0.89445	0.65501	0.94	0.947
5	Row 1 SB, Ax	0.67032	0.45834	0.38023	0.85206	0.576
6	Row 1 SB, Az	0.55136	0.24041	0.4763	0.66014	0.633
5	Row 2 Port, Ax	0.76629	0.62429	0.32518	0.998	0.677
6	Row 2 Port, Az	0.58338	0.0.18592	0.28122	0.92403	0.586
7	Row 2 SB, Ax	0.71035	0.56112	0.28189	0.89604	0.617
8	Row 2 SB, Az	0.2358	0.025653	0.39651	0.11236	0.458
9	Row 3 Port, Ax	0.66082	0.45191	0.33539	0.60816	0.639
10	Row 3 Port, Az	0.56286	0.00418	0.49035	0.92003	0.648
11	Row 3 SB, Az	0.5676	0	0.49121	0.968	0.642
12	Row 5 Port, Ax	0.7188	0.6384	0.3784	0.7961	0.703
13	Row 5 Port, Az	0.5855	0.3028	0.2835	0.7621	0.595
14	Row 5 SB, Ax	0.608	0.4823	0.3482	0.4922	0.653
15	Row 5 SB, Az	0.7087	0.463	0.4724	0.986	0.713
16	Row 6 Port, Ax	0.72193	0.4764	0.3841	0.7901	0.685
17	Row 6 Port, Az	0.5673	0.3274	0.4312	0.6501	0.59
18	Row 6 SB, Ax	0.7837	0.5508	0.3471	0.908	0.7
19	Row 8 SB, Ax	0.749	0.5512	0.359	0.948	0.67
20	Row 8 SB, Az	0.441	0.0173	0.2822	0.4802	0.619
21	Row 9 Port, Ax	0.67204	0.44	0.2888	0.8321	0.594
22	Row 9 Port, Az	0.5184	0	0.2024	0.976	0.471
23	Row 9 SB, Ax	0.5942	0	0.4788	0.7941	0.585
24	Row 9 SB, Az	0.525	0.256	0.2605	0.738	0.485
25	Row 10 Port, Ax	0.6592	0.4398	0	0.84	0.612
26	Row 10 Port, Az	0.3435	0	0	0.2863	0.493
27	Row 12 SB, Ax	0.7422	0.48	0.3047	0.898	0.622

Test-Analysis Comparisons for Airframe/Floor Intersections						
28	Port Frame FS 2200, Ax	0.6537	0.3402	0.2295	0.948	0.596
29	Port Frame FS 2200, Az	0.5123	0.1357	0	0.72	0.566
30	SB Frame FS 3050, Ax	0.6697	0.33	0.07591	0.994	0.627
31	SB Frame FS 3050, Az	0.595	0.18895	0.1343	0.8721	0.624
32	Port Frame FS 6805, Ax	0.6666	0.4798	0.4353	0.726	0.612
33	Port Frame FS 6805, Az	0.6382	0.3421	0	0.964	0.584
34	SB Frame FS 6305, Ax	0.7087	0.3616	0	0.974	0.668
35	SB Frame FS 6305, Az	0.5689	0.115	0	0.968	0.543
36	Port Frame FS 7805, Ax	0.6631	0.427	0.469	0.7341	0.621
37	Port Frame FS 7805, Az	0.5044	0	0	0.936	0.503
38	SB Frame FS 7305, Ax	0.6207	0.313	0.3524	0.6322	0.635
39	SB Frame FS 7305, Az	0.5767	0.168	0	0.952	0.556
40	Port Frame FS 8805, Ax	0.6998	0.533	0.2594	0.8561	0.648
41	Port Frame FS 8805, Az	0.7362	0.5932	0.2354	0.906	0.667
42	SB Frame FS 8305, Ax	0.6954	0.2779	0.4577	0.924	0.594
43	SB Frame FS 8305, Az	0.5865	0.1984	0	0.946	0.553
44	Port Frame FS 9805, Ax	0.7094	0.5373	0.272	0.8781	0.704
45	Port Frame FS 9805, Az	0.7036	0.5238	0.246	0.924	0.681
46	SB Frame FS 9305, Ax	0.6118	0.492	0.357	0.5262	0.659
47	SB Frame FS 9305, Az	0.6596	0.4548	0.1314	0.8721	0.628
48	Port Frame FS 10790, Ax	0.6334	0.4831	0.0316	0.7841	0.616
49	Port Frame FS 10790, Az	0.6881	0.5937	0.223	0.8681	0.659
50	SB Frame FS 10305, Ax	0.5358	0.252	0.29	0.938	0.491
51	SB Frame FS 10305, Az	0.6377	0.3729	0.0601	0.898	0.619
52	Port Frame FS 11905, Ax	0.6996	0.5379	0	0.914	0.67
53	Port Frame FS 11905, Az	0.643	0.5078	0.24	0.882	0.626
54	SB Frame FS 11405, Ax	0.6389	0.403	0.005	0.916	0.606
55	SB Frame FS 11405, Az	0.715	0.4848	0	0.916	0.733
56	Port Frame FS 12875, Ax	0.6673	0.487	0	0.96	0.592
57	Port Frame FS 12875, Az	0.5535	0.311	0	0.8781	0.521
58	SB Frame FS 13345, Ax	0.671	0.4131	0	0.974	0.614
59	SB Frame FS 13345, Az	0.6061	0.321	0.05123	0.926	0.529
Test-Analysis Comparison of Discrete Airframe Locations						
60	Nose Cone Bulkhead, Ax	0.5147	0	0	0.5462	0.628
61	Nose Cone Bulkhead, Az	0.5292	0.0665	0	0.952	0.56
62	Port Engine Nacelle, Ax	0.4926	0.222	0.0273	0.7641	0.518
63	Port Engine Nacelle, Az	0.6611	0.4644	0.404	0.934	0.634
64	SB Engine Nacelle, Ax	0.5551	0.439	0.141	0.6082	0.566
65	SB Engine Nacelle, Az	0.45956	0.1884	0.3941	0.642	0.543
66	Tail, Ax	0.5785	0.2844	0.4482	0.9678	0.566
67	Tail, Az	0.4701	0.1813	0.5407	0.7378	0.479

6.0 CONCLUSIONS

A full-scale crash test of a Fokker F28 regional jet was conducted at NASA Langley's Landing and Impact Research Facility. The test was performed under a cooperative research agreement between the FAA and NASA and the test objectives were to provide data for assessment of transport aircraft crashworthiness under realistic impact conditions and to generate test data for model validation. A LS-DYNA finite element model of the aircraft was developed, based on a NASTRAN loads model obtained from Fokker at the same time that the hardware was purchased. Test-analysis comparisons were made in several categories including inertial properties, kinematic assessments, structural responses of the seat bases and the airframe/floor intersections, and comparison of airframe deformation and failure. In addition, the ISO/TR 16250 standard was applied to assess test-analysis correlation.

Findings of this research effort are listed as follows:

(1) Inertial properties of the test article and finite element model were matched within 6.6%.
(2) Kinematic comparisons, including comparisons of forward and vertical velocity responses of photogrammetric test data and model predictions, were in excellent agreement.
(3) Test-analysis comparisons of acceleration responses showed a wide range of agreement. The predicted responses at the pilot seat showed excellent comparison with test. In addition, vertical acceleration responses were generally better predicted than the forward responses.
(4) The ISO/TR-16250 curve comparison methodology was applied to all structural time history responses presented in the paper. In particular, the combined ISO rating, R, was examined, which ranges from 0 to 1.0, with higher scores indicating better agreement. None of the test-analysis curves exhibited excellent correlation and only one channel (pilot seat vertical velocity) exhibited good correlation. Forty-six of sixty-seven channels demonstrated fair agreement, while the remaining channels had poor agreement. If 0.5 is applied as the delimiter for this correlation study, then 62 of 67 test-analysis responses would be deemed adequate.

7.0 REFERENCES

1. ***Federal Register***. Federal Aviation Administration, Aviation Rulemaking Advisory Committee, Transport Airplane and Engine Issues, Vol 80. 2015.

2. Jones L. E., "Overview of the NASA Systems Approach to Crashworthiness Program," Proceedings of the American Helicopter Society 58th Annual Forum, Montreal Canada, June 11-13, 2002.

3. Pretson G. M. and Pesman, G. J. "Accelerations in Transport-Airplane Crashes." NASA TN-4158. 1958.

4. Abramowitz A. et al. "Vertical Drop Test of an ATR 42-300 Airplane." DOT/FAA/AR-05/56.

5. Jackson K. E., and Fasanella E. L., “Development and Validation of a Finite Element Simulation of a Vertical Drop Test of an ATR-42 Regional Transport Airplane,” DOT/FAA/AR-08/19, June 2008.

6. McGuire R. J. et al. “Vertical Drop Test of a Metro III Aircraft,” DOT/FAA/CT-93/1.

7. McGuire R. J. et al. “Vertical Drop Test of a Beechcraft 1900C Airliner.” DOT/FAA/AR-96/119.

8. Abramowitz A. et al. “Vertical Drop Test of a Shorts 3-30 Airplane.” DOT/FAA/AR-99/87.

9. Hayduk R. J. “Full-Scale Transport Controlled Impact Demonstration.” Proceedings of a workshop sponsored by NASA Langley Research Center and FAA Technical Center. NASA CP-2395. 1985.

10. Fasanella E. L. et al. “Impact Data from a Transport Aircraft During a Controlled Impact Demonstration.” NASA-TP-2589. 1986.

11. Williams M. S., and Hayduk, R. J., "Vertical Drop Test of a Transport Fuselage Section Located Forward of the Wing," NASA TM-85679, 1983.

12. Fasanella E. L., and Alfaro-Bou, E., "Vertical Drop Test of a Transport Fuselage Section Located Aft of the Wing," NASA TM-89025, 1986.

13. Williams M. S., and Hayduk, R. J., "Vertical Drop Test of a Transport Fuselage Center Section Including the Wheel Wells," NASA TM-85706, October 1983.

14. Barth T. H. “Discovery Channel Plane Crash.” Proceedings from the Seventh Triennial Fire and Cabin Safety Conference. December 3, 2016.

15. Vaughan V. L., Alfaro-Bou E., “Impact Dynamics Research Facility for Full-Scale Aircraft Crash Testing,” NASA-TN-8179, April 1976.

16. Lyle K. H., Stockwell A. E., and Hardy R. C. “Application of Probability Methods to Assess Airframe Crash Modeling Uncertainty,” ***Journal of Aircraft***, Vol. 44, No. 5, September-October 2007, pp. 1568-1573.

17. Stockwell A. E., “Fokker F28 Fuselage Section Drop Test Simulation and Test/Analysis Correlation,” Report No. SDSR-07RCG-093003, 2003, Lockheed Martin Company, Langley Program Office, Hampton, VA.

18. Jackson K. E., Littell J. D., Annett M. S. and Haskin I. M., "Vertical Drop Test and Simulation of a Fokker F-28 Fuselage Section," Proceedings of the ASCE 2018 Earth and Space Conference, Cleveland, OH, April 11-13, 2018.

19. Jackson K.E., Littell J. D., Annett M. S. and Haskin I. M., "Finite Element Simulations of Two Vertical Drop Tests of F-28 Fuselage Sections," NASA Technical Memorandum NASA/TM-2018-219807, February 2018.

20. Littell J. D. "Full Scale Drop Test of a Fokker F28 Forward Fuselage Section onto Soil," Proceedings of the Aerospace Structural Impact Dynamics International Conference, Wichita, KS, October 17-19, 2017.

21. Littell J. D. "Full-Scale Drop Test of a Fokker F28 Wing-Box Fuselage Section," Proceedings of the 16th Biennial ASCE Earth and Space Conference, Cleveland, OH, April 9-12, 2018.

22. Baker W., Untaroiu C. and Chowdhury M., "Development of a Finite Element Model of the WIAMAN Lower Extremity to Investigate Under-Body Blast Loads," Proceedings of the 14th International LS-DYNA Users Conference, Dearborn, MI, 2016.

23. Shaw G., Crandall J., and Butcher J., "Comparative Evaluation of the THOR Advanced Frontal Crash Test Dummy," ***International Journal of Crashworthiness***, Volume 7, 2002, Issue 3, pp. 239-254.

24. International Standards Organization (ISO) Technical Report, "Road vehicles - Objective rating metrics for dynamic systems," ISO/TR 16250, July 15, 2013.

25. Littell J. D., "A Summary of Results from Two Full-Scale Fokker F28 Fuselage Section Drop Tests," NASA/TM-2018-219829, May 2018.

26. Littell J. D., "Experimental Photogrammetric Techniques Used on Five Full-Scale Aircraft Crash Tests," NASA TM-2016-219168, March 2016.

27. Littell J. D., "Large Field Digital Image Correlation used for Full-Scale Crash Testing: Methods and Results," Proceedings of the Society of Experimental Mechanics International Digital Image Correlation Fall Conference, Philadelphia, PA, November 2016.

28. Littell J. D., "A Summary of Airframe Results from a Fokker F-28 Full-Scale Crash Test," to be published as a NASA Technical Memorandum, expected March 2020.

29. Anon. "MSC/NASTRAN Quick Reference Guide," Version 70.5, The MacNeal-Schwendler Corporation, Los Angeles, CA, February 1998.

30. Hallquist J. O. "LS-DYNA Keyword User's Manual," Volume I, Version 971, Livermore Software Technology Company, Livermore, CA, 2006.

31. Hallquist J. O. "LS-DYNA Keyword User's Manual," Volume II Material Models, Version 971, Livermore Software Technology Company, Livermore, CA, August 2006.

32. Hallquist J. O. "LS-DYNA Theory Manual," Livermore Software Technology Company, Livermore, CA, March 2006.

33. Thomas M. A., Chitty D. E., Gildea M. L. T'Kint C. M., "Constitute Soil Properties for Unwashed Sand and Kennedy Space Center," NASA CR-2008-215334, 2008.

34. Fasanella E. L., Jackson K. E., and Kellas S., "Soft Soil Impact Testing and Simulation of Aerospace Structures," Proceedings of the Tenth International LS-DYNA Users Conf., Dearborn, MI, June 8-10, 2008.

35. Thomas M. A., Chitty D. E., Gildea M. L. T'Kint C. M., "Constitutive Soil Properties for Cuddeback Lake, California and Carson Sink, Nevada," NASA/CR-2008-215345, August 2008.

36. Mark S. D., "Orion Landing Simulation Eight Soil Model Comparisons," NASA/CR-2009-215757, June 2009.

37. Putnam J. B. and Jackson K. E., "Simulation of Occupant Response within a Full-Scale Crash Test of a Fokker F28 Fellowship Aircraft," NASA Technical Memorandum, expected March 2020.

38. ABAQUS-Explicit (2012). ABAQUS User's Manual, Volume III, Version 6.12, Dassault Systèmes, Simulia Corporation, Pawtucket, RI.

39. PAM-CRASH (2003). Virtual Prototyping Software and Solutions, ESI-Group.

40. RADIOSS 2017 Reference Manual Documents, User Guide and Tutorials, Altair, Troy, MI.

41. Jiang X. and Mahadevan S., "Bayesian risk-based decision method for model validation under uncertainty," ***Reliability Engineering of System Safety***, 2007, Vol 92, No. 6, pp.707-718.

42. Jiang X., and Mahadevan S., "Bayesian wavelet method for multivariate model assessment of dynamical systems," ***Journal of Sound and Vibration.*** 2008, Vol 312 **(4-5**) pp. 694–712.

43. Jiang X., Yang R. J., Barbat S ., Weerappuli P., "Bayesian probabilistic PCA approach for model validation of dynamic systems," ***SAE International Journal of Materials and Manufacturing***, 2009, Vol. 2, No. 1, pp. 555-563.

44. Mongiardini M., Ray M.H., Anghileri M. (2009) "Development of a Software for the Comparison of Curves During the Verification and Validation of Numerical Models," Proceedings of the 7th European LS-DYNA Conference, Salzburg, Austria, May 14-15.

45. Schwer L. E., "Validation metrics for response histories: perspectives and case studies," ***Engineering with Computer***, 2007, Vol 23, pp. 295-309.

46. Sprague M. A., and Geers T. L., "Spectral Elements and Field Separation for an Acoustic Fluid Subject to Cavitation," ***Journal of Computational Physics***, Vol. 184, 2003, pp: 149-162.

47. Thunert C., "Manual of the program CORA," Version 3.5"; GNS mbH; Braunschweig, Germany, 2010.

48. Thunert C., "CORA Release 3.6 – User's Manual"; GNS mbH; Braunschweig, Germany, 2012.

49. **S**arin H., Kokkolaras M., Hulbert G., Papalambros P., Barbat S., Yang R. J., "A Comprehensive Metric for Comparing Time Histories in Validation of Simulation Models with Emphasis on Vehicle Safety Applications," ***Transactions of the ASME – Journal of Dynamic Systems: Measurement and Control***; 132(6), 061401;USA, 2010.

50. Zhan Z., Fu Y., Yang R.J., "Enhanced Error Assessment of Response Time Histories (EEARTH) Metric and Calibration Process," SAE 2011 World Congress, SAE2011-01-0245, Detroit, MI, 2011.

51. Mahadevan S., and Rebba R., "Validation of reliability computational models using Bayes networks," ***Reliability Engineering of System Safety***, 2005, 87 (2) pp. 223–232.

52. **R**ebba R. and Mahadevan S., "Model predictive capability assessment under uncertainty," ***AIAA Journal***, 2006, Vol. 44, No. 10, pp. 2376–2384.

53. Zhan Z., Fu Y., Yang R. J., Peng Y., "Development and Application of a Reliability-Based Multivariate Model Validation Method," ***Int. J. Veh. Des.*** 2012, 60 (3/4) pp. 194–205.

54. Jiang X., Yang R. J., Barbat S., Weerappuli P., "Bayesian probabilistic PCA approach for model validation of dynamic systems," *SAE International Journal of Materials & Manufacturing*, 2009, Vol 2, No. 1, pp. 555-563.

55. Kass R. and Raftery A., "Bayes factors," ***Journal of the American Statistical Association***, 1995, Vol 90 (430), pp. 773–795.

56. Zhan Z., Fu Y., Yang R. J., Peng Y., "An Enhanced Bayesian Based Model Validation Method for Dynamic Systems," ***ASME Journal of Mechanical Design***, 2011, 133(4), 041005.

57. NESC-RP-13-00876, "Analysis of Anthropomorphic Test Device (ATD) Response for Proposed Orion Crew Impact Attenuation System (CIAS)," 2016.

REPORT DOCUMENTATION PAGE

Form Approved
OMB No. 0704-0188

1. REPORT DATE *(DD-MM-YYYY)*
1-02-2020

2. REPORT TYPE
Technical Memorandum

3. DATES COVERED *(From - To)*

4. TITLE AND SUBTITLE
Simulation of a Full-Scale Crash Test of a Fokker F28 Fellowship Aircraft

5a. CONTRACT NUMBER

5b. GRANT NUMBER

5c. PROGRAM ELEMENT NUMBER

6. AUTHOR(S)
Jackson, Karen E.; Putnam, Jacob B.

5d. PROJECT NUMBER

5e. TASK NUMBER

5f. WORK UNIT NUMBER
664817.02.07.03.03.02

7. PERFORMING ORGANIZATION NAME(S) AND ADDRESS(ES)
NASA Langley Research Center
Hampton, VA 23681-2199

8. PERFORMING ORGANIZATION REPORT NUMBER
L-21096

9. SPONSORING/MONITORING AGENCY NAME(S) AND ADDRESS(ES)
National Aeronautics and Space Administration
Washington, DC 20546-0001

10. SPONSOR/MONITOR'S ACRONYM(S)
NASA

11. SPONSOR/MONITOR'S REPORT NUMBER(S)
NASA-TM-2020-220435

12. DISTRIBUTION/AVAILABILITY STATEMENT
Unclassified-
Subject Category 39
Availability: NASA STI Program (757) 864-9658

13. SUPPLEMENTARY NOTES

14. ABSTRACT In June 2019, a full-scale crash test of a Fokker F28 Fellowship aircraft was conducted as part of a joint National Aeronautics and Space Administration/Federal Aviation Administration (NASA/FAA) project to investigate the performance of transport aircraft under realistic crash conditions. The test objectives were to provide data for assessment of transport aircraft crashworthiness and to generate test data for model validation. The test article was loaded with transport aircraft seats in a 3+2 configuration. A total of 24 instrumented Anthropomorphic Test Devices (ATDs) were placed in the seats and restrained. The test article weighed 33,306-lb. and, during the crash test, impacted a 2-ft. high soil bed at 65.3-ft/s forward and 31.8-ft/s vertical velocity. The full-scale crash test was simulated using the commercial nonlinear explicit transient dynamic finite element code, LS-DYNA¿. This paper will provide a description of the test article and the crash test conditions, document the F28 full-scale model development, and present test-analysis comparisons in several categories including inertial properties, kinematic responses, structural acceleration responses, and airframe deformation and failure. In addition, test-analysis results will be quantified based on the International Organization for Standardization (ISO) 16250 curve comparison methodology.

15. SUBJECT TERMS
Crash impact simulation; LS-DYNA; test-analysis corelation

16. SECURITY CLASSIFICATION OF:			17. LIMITATION OF ABSTRACT	18. NUMBER OF PAGES	19a. NAME OF RESPONSIBLE PERSON
a. REPORT	b. ABSTRACT	c. THIS PAGE			STI Help Desk (email: help@sti.nasa.gov)
U	U	U	UU	46	19b. TELEPHONE NUMBER *(Include area code)* (757) 864-9658